Electronic ISSN: 1309-0267

International Journal of Engineering & Applied Sciences

IJEAS

I J E A S

Volume 11, Issue 1
2019

Published by Akdeniz University

Editorial Board

(The name listed below is not Alphabetical or any title scale)

Abstracting & Indexing

IJEAS provides unique **DOI** link to every paper published.

Editorial Scope

The journal presents its readers with broad coverage across some branches of engineering and science of the latest development and application of new solution algorithms, artificial intelligent techniques innovative numerical methods and/or solution techniques directed at the utilization of computational methods in solid and nano-scaled mechanics.

International Journal of Engineering & Applied Sciences (IJEAS) is an Open Access Journal

International Journal of Engineering & Applied Sciences (IJEAS) publish original contributions on the following topics:

Numerical Methods in Solid Mechanics

Nanomechanic and applications

Microelectromechanical systems (MEMS)

Vibration Problems in Engineering

Higher order elasticity (Strain gradient, couple stress, surface elasticity, nonlocal elasticity)

Applied Mathematics

CONTENTS

International Journal of Engineering & Applied Sciences (IJEAS)
Vol.11, Issue 1 (2019) 310-329
http://dx.doi.org/10.24107/ijeas.531011
Int J Eng Appl Sci 11(1) (2019) 310-329

Modeling and Buckling Analysis of Rectangular Plates in ANSYS

Ahmed Hassan Ahmed Hassan [a], Naci Kurgan [b]*

[a,b] Ondokuz Mayis University, Faculty of Engineering, Department of Mechanical Engineering, Samsun, Turkey.
E-mail address: 15210457@stu.omu.edu.tr [a*], naci.kurgan@omu.edu.tr [b]

ORCID numbers of authors:
0000-0002-4880-0184 [a], 0000-0001-7297-7249 [b]*

Received date: 22.02.2019
Accepted date: 19.04.2019

Abstract

With plate-buckling problem still being an active area of research in the field of mechanics of materials, researchers need to validate the proposed solutions and theories, using analysis tools such like ANSYS, which is a robust general-purpose finite element analysis tool. This article investigates modeling and buckling analysis of rectangular plates in ANSYS® Mechanical APDL, Release 17.1, through a series of comparative studies conducted on various models and options. Shell and solid models of homogeneous and functionally graded plate (FGP) using various elements are investigated. Expressing boundary conditions on both shell and solid models of plate for buckling analysis is discussed. Procedures of buckling analysis in ANSYS are presented and effects of meshing, boundary conditions and element options are examined though comparative studies. Results obtained from ANSYS are compared to various analytical solutions.

Keywords: Plate buckling; ANSYS; functionally graded; shell models; solid models.

1. Introduction

Reddy defines plate as: *"A plate is a structural element with planform dimensions that are large compared to its thickness and is subjected to loads that cause bending deformation in addition to stretching* [1]*"*. Plate may be rectangular, square, circular, skew or any other geometry with or without holes. Due to its relative simplicity and wide application, rectangular plate is usually used to illustrate the plate definition [1-4]. A rectangular plate is shown in Fig. 1 with typical coordinate system and names of characteristic dimensions. Normally, the length of the plate is referred to as (a) and the width is referred to as (b) while the thickness is referred to as (h).

In the applications that flat plate experiences in-plane compression, buckling phenomenon may occur. Buckling of a plate is defined as the loss of its stability under compressive loading [5]. Loss of stability means that shape of the buckled structure changes into a different configuration when the loads reach a critical value. Buckling occurrence depends on the shape of the structure, properties of the material, loading configuration and boundary conditions. Different bodies buckle in different ways. Flat plates experience bifurcation buckling, aka classical buckling [2]. Many analysis procedures have been proposed to solve the problem of plate buckling. One of

the most used method in structural engineering is the finite element analysis (FEA). That is due to its profound theory and its ability to analyse complicated geometries and include nonlinearities. ANSYS® provides a ready-to-use general-purpose FEA software that has the capability of coupling different analysis fields. A plate can be modeled in ANSYS in many ways.

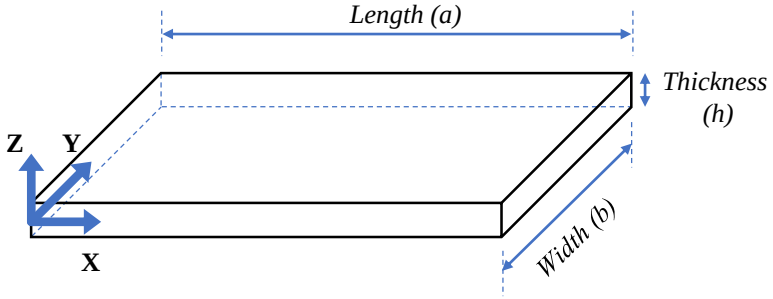

Fig. 1. Rectangular plate structure

Countless articles use ANSYS for performing buckling analyses on plates as a verification step for their presented methods, but with no intension to share the models, options or steps used in the ANSYS analysis. Few articles consider sharing or conducting whole research on models and options of specific analysis type within some analysis software. An example for such efforts is the recently published article by Mercan [6], who presented a demonstration of how to mesh and prepare micro and nano sized structures using some analysis software package.

This article investigates plate modeling and buckling analysis and compares models to each and to plate theories aiming at being a reference that guides researchers in choosing plate models for buckling analysis. Effects of mesh size, number of layers and options of elements are also presented. In literature, various plate models in ANSYS are compared based on modal and stress analyses; but there is no reference found that could be a guide for researchers to conduct buckling analysis on rectangular plates in ANSYS. This kind of reference exists only for stress and modal analyses. Banerjee [7] compared between a plate models of shell elements and solid-shell elements for stress analysis. Wang [8] compared between plate models of shell, solid and solid-shell elements for stress and modal analysis. For buckling analysis, Swamy [9] presented buckling of rectangular plate using legacy planar element. Buckling of cylindrical thin-walled structures was presented by Subramani [10], who compared between two shell models, and Bischoff [11] who compared a shell and a solid models in ANSYS.

This article presents rectangular plate modelling and buckling analyses in ANSYS. Effects of mesh size, number of layers and options of elements are also presented. The process of obtaining results from analyses of many different models was automated using APDL, which is a scripting language that can be used within ANSYS [12]. The version of ANSYS used in this research is ANSYS® Mechanical APDL, Release 17.1.

2. ANSYS elements used in plate models

ANSYS provides wide range of groups of elements covering many simulation fields. For rectangular plate models, shell, solid and solid-shell elements are used in this article.

2.1. Shell elements

Shell elements that are suitable to model rectangular plates are *Shell181* [13] and *Shell281* [14]. Shell elements simulate the concept of plate/shell theories, which reduce the plate problem to surface model with strain/deformation assumptions through the thickness. Structural shell elements available in ANSYS are based on first-order shear-deformation theory (FSDT), and they can model homogeneous as well as laminated plates by using the ANSYS command SECDATA [15].

2.2. Solid elements

Solid elements are used to model the plate as three-dimensional solid body. Although using these elements seems to be modeling the exact plate, it experiences "locking" problems when simulating thin plates. Locking phenomenon is related to the finite elements methods, makes the model behave different from what it should be [1]. Therefore, using solid elements in modeling thin plates should be associated with some treatment of the results. Solid structural elements in ANSYS can be classified into tetrahedral and brick elements.

2.2.1 Tetrahedral elements

Tetrahedral elements include *Solid285* [16] and *Solid187* [17]. Tetrahedral elements have a high capability to model irregular meshes. These elements can be used to model homogeneous plates, but there is no ready tool to model laminated plates using these elements in ANSYS. One have to assign different materials to different layers through thickness, or glue different adjacent volumes of different materials together in order to model a laminated plate.

2.2.2 Brick elements

Brick elements include *Solid185* [18] and *Solid186* [19]. In their brick form, they lack the high capability of tetrahedral elements of modeling irregular meshes. However, for regular geometry, they provide more accurate results than tetrahedral elements. Laminated plates can be modeled as adjacent layers of brick elements assigned with different materials. In addition, brick structural elements provided by ANSYS have the ability to be associated with a shell section; meaning that different materials can be assigned to different sections through the thickness of a plate by using the ANSYS command SECDATA. Therefore, laminated plates can be also modeled directly using available section commands in ANSYS.

2.3. Solid-shell element

There is only one solid-shell element provided in ANSYS; called *Solsh190* [20]. Solid-shell elements are relatively a recent technology that intends to combine the benefits of solid elements and shell elements at once. *Solsh190* is a brick structural element with the ability to include strain assumptions, which are intended to prevent various forms of locking phenomenon when modeling thin plates while being able to model thick plates accurately as well.

3. Boundary conditions

Boundary of a plate, i.e. edge, may have free, clamped or simply supported boundary condition [1]. Other less common boundary conditions include hinged, fixed and sliding edges. For buckling analysis, boundary conditions have to allow displacement at least in the direction in

which load acts. Main boundary conditions of a plate under buckling analysis should interrupted as follows:

a) **Free edge (F):** is not geometrically restrained in any way.
b) **Simply supported edge (SS):** is free to have inplane displacements and rotates freely about its axis. This is the basic meaning of simply supported edge. Additional conditions might be added to this boundary condition, like being inextensible or immovable, also called SS-1 and SS-2, respectively.
c) **Clamped edge (C):** is free to have only inplane displacements.
d) **Fixed edge:** is a fully restrained edge. Neither rotations nor displacements are allowed.

Modeling geometry and boundary conditions of a rectangular flat plate for buckling analysis in ANSYS is discussed as follows.

3.1. Modeling plate and boundary conditions in ANSYS

In ANSYS, plate can be modeled as shell model or solid model. Boundary conditions expressed as displacement constraints, i.e. essential primary boundary conditions. Depending on the considered plate model, boundary conditions may be expressed as follows.

3.1.1 Shell models

Shell models are based on the shell elements *Shell181* or *Shell281*. Plate shell model is an area meshed into smaller areas of shell elements. Shell elements have translation (UX, UY and UZ) and rotation (ROTX, ROTY and ROTZ) degrees of freedom at their nodes. Two important notes have to be considered about the implications of boundary conditions on those degrees of freedom. Firstly, rotation of edge about the thickness direction (UZ) is actually the inplane displacements (UX and UY). Therefore, restraining of ROTZ implies restraining of inplane displacements In other words, if inplane displacements (UX and UY) are to be allowable, ROTZ has to be allowable too. Secondly, rotation of edge about an inplane axis perpendicular to the edge actually means the out-of-plane displacement. Fig. 2 shows various boundary conditions expressed on shell model of a plate with two edges simply supported, one clamped and the last is free.

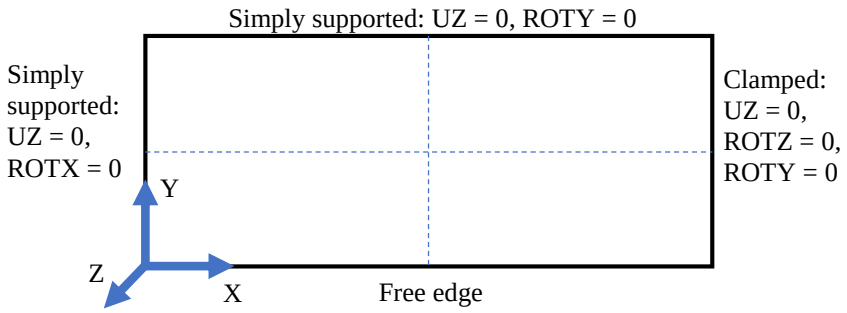

Fig. 2. Boundary conditions on shell model of plate

3.1.2 Solid models

Solid models are based on solid or solid-shell elements (*Solid185*, *Solid186*, *Solid187*, *Solid285* or *Solsh190*). Plate solid model is a solid body meshed into small volumes of solid elements. Solid elements have only translation (UX, UY and UZ) degrees of freedom at their nodes. Boundary conditions on solid model are expressed on faces of the edges. For instance, simply

supported edge in solid model is an edge that all nodes on the face of that edge have no lateral displacement allowed. Since no rotational degree of freedom available for solid elements, clamped boundary condition is expressed by coupling all nodes on the clamped edge's face in its normal direction. This prevents the edge from rotating around its axis. Fig. 3 shows various boundary conditions expressed on solid model of plate.

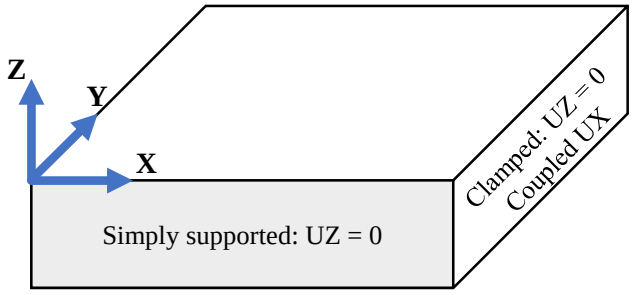

Fig. 3. Boundary conditions on solid model of plate

3.2. Plate model symmetry and anti-symmetry

Although some plate problems may have symmetry/anti-symmetry in geometry, loads and boundary conditions, expression symmetry/anti-symmetry in ANSYS for plate buckling analysis has to be done with attention. When imposing symmetry/anti-symmetry in the analysis, some buckling modes may be missed because only symmetric/anti-symmetric modes will be calculated. Therefore, it is advisable to work with full model whenever possible to ensure that no buckling mode has been missed. Fig. 4 shows full and symmetry models of a fully simply supported plate, i.e. all edges are simply supported, under uniaxial uniform pressure P expressed as load per unit length of the edge.

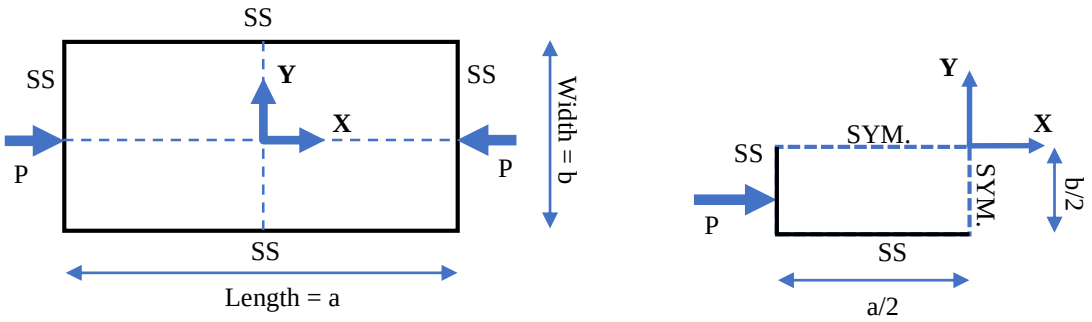

a) Full model b) Symmetry model

Fig. 4. Full (a) and Symmetry (b) models of simply supported plate under uniaxial pressure

To further illustrate the behavior of symmetry model compared to full model a thin plate of length 1.5 m, width 1 m, and thickness 2 mm under uniaxial uniform pressure acting on the shorter edges, is modeled as full plate Fig. 4-a, and as symmetry model Fig. 4-b and linear eigenvalue buckling analysis is conducted. Elasticity modulus is assumed as 70 GPa and Poisson's ratio as 0.3. As shown in

Fig. 5, by using symmetry model ANSYS calculated first buckling load as 2.378 N/mm, while for the full model the first buckling load is calculated as 2.199 N/mm as shown in

Fig. 6-a. Here the symmetry model has missed the first buckling load. The buckling load calculated using the symmetry model is actually the second buckling load for the full model as shown in

Fig. 6-b.

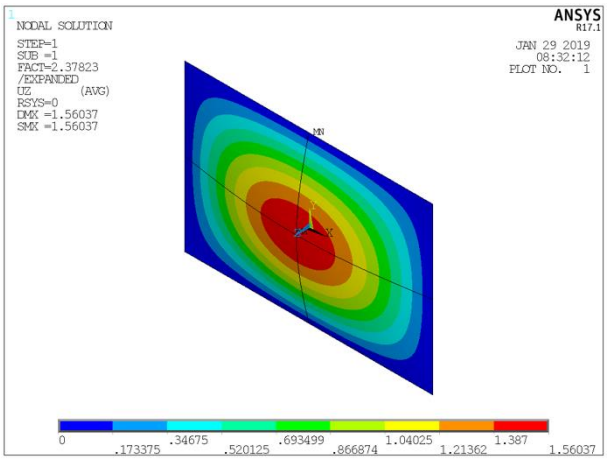

Fig. 5. First buckling mode of the symmetry model, buckling factor = 2.37823

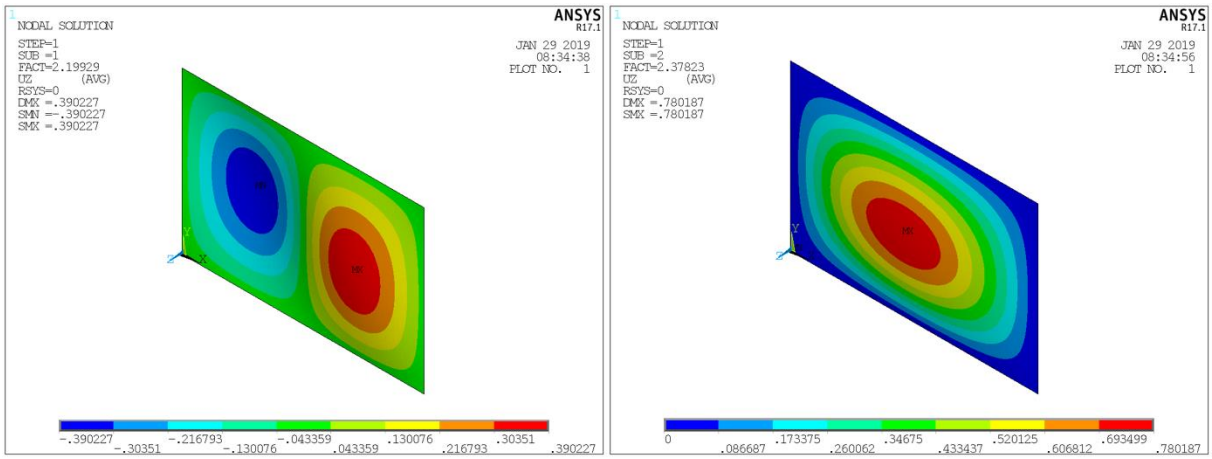

a) 1st buckling mode, buckling factor = 2.19929

b) 2nd buckling mode, buckling factor = 2.37823

Fig. 6. First (a) and second (b) buckling modes of the full model

3.3. Additional consideration for boundary conditions in ANSYS

In spite of plate being under balanced forces, the model may need additional boundary conditions to restrain the rigid body translation and rotation. For example, for a full plate model with all edges being simply supported, additional constrains need to be added in order to prevent rigid body movement. In general, constraining of two different points in the plate should be enough to achieve prevention of rigid body movement under any loading/boundary conditions configuration.

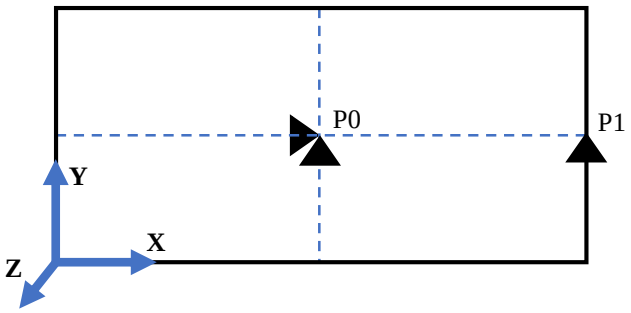

Fig. 7. Additional conditions for full shell model of plate

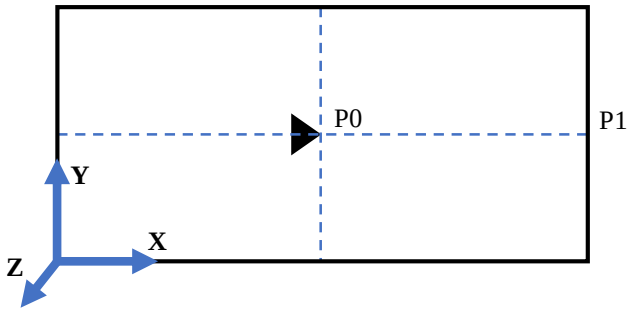

Fig. 7 shows a typical configuration of additional constraints for a full shell model. Point P0 is restrained in X and Y directions, while point P1 is restrained in Y direction.

4. Buckling analysis in ANSYS

In ANSYS, buckling analysis might be conducted using Eigenvalue buckling analysis or nonlinear static analysis [21]. Eigenvalue buckling analysis reveals the buckling load factor that has to be multiplied by the applied loads to reach buckling point [22, 23]. Eigenvalue buckling analysis may be based on linear or nonlinear static analysis. Linear eigenvalue buckling analysis deals with ideal elastic structure and provides a non-conservative estimation that is useful for later complicated nonlinear buckling analyses. ANSYS provides a ready-to-use tool for eigenvalue buckling analysis and calculates buckling load factor along with buckling mode shapes. Note that displacements shown by ANSYS in these analyses have no physical meaning by themselves, and they are only useful in showing the buckling mode shape.

The second way to conduct buckling analysis in ANSYS is through a nonlinear static structural analysis [24, 25], which is a static analysis with large displacement option enabled. Plate is put under incremental load that is greater than estimated buckling load, and then the load-deflection curve is examined for the bifurcation point. The bifurcation point is the point at which the response (deflection in lateral direction, UZ) suddenly changes more rapidly, i.e. buckling point. Various nonlinearities and imperfections can be included in the nonlinear analysis. Attention must be paid when conducting buckling analysis of homogeneous or symmetric laminated plate under only inplane loads; because buckling behavior would not captured by ANSYS. In this case, initial imperfection is needed to establish a deflection that will then get increasing with the increasing load and monitored for the buckling point. This initial imperfection is expressed usually as initial deformation obtained from previous static analysis for the plate under lateral loads, or from buckling mode shape resulted from previous buckling analysis. The imposed initial imperfection has to be small enough in order to obtain a curve with noticeable bifurcation point. Fig. 8 compares two load - lateral displacement (UZ) curves,

i.e. load-deflection curves, of the mid-point of a plate, resulted from nonlinear statics structural analysis under same boundary conditions and loads with two different initial deflections.

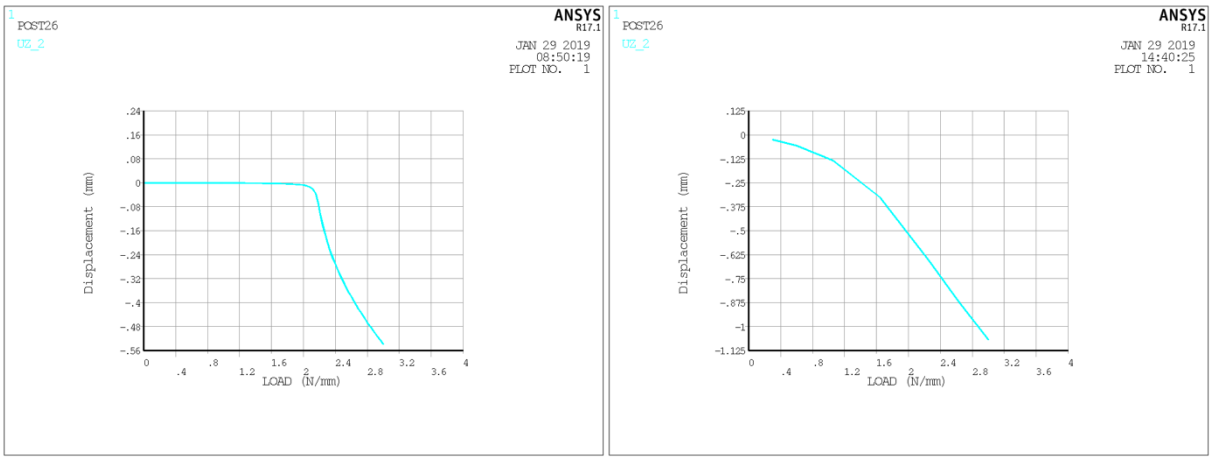

a) Small initial deflection b) Large initial deflection

Fig. 8. Load-Lateral Displacement curves of plate with (a) slight and (b) larger initial deflection

Results shown in Fig. 8 are for a plate of 1.5m length, 1m width and 2mm thickness, with 70 GPa elasticity modulus and 0.3 Poisson's ratio, under uniaxial uniform pressure acting on the shorter edges. Initial deflected geometries were obtained from previous linear eigenvalue buckling analysis, shown in

Fig. 6-a with updating geometry using UPGEOM [15] ANSYS command with small factor for the first analysis, and relatively larger factor for the second. For the first case, a bifurcation point can be observed through its load-deflection curve, while this is not the case for the second. By checking Fig. 8-a, it can be seen that buckling load is roughly 2.2 N/mm, which is same as the one obtained using eigenvalue buckling analysis tool that shown in

Fig. 6-a. Imposing even smaller initial deflection leads to clearer bifurcation point.

5. Meshing

Finite element analysis (FEA) is based on the concept of discretization of the region of the problem to smaller simpler elements; which are then solves and reassembled obtain a solution of the problem. This discretizing process is called meshing. Mesh size affects the accuracy of the solution. When modeling a plate in ANSYS, as in every FEA tool, one must decide a suitable mesh size for the elements. Smaller mesh size generates more elements and results that are more accurate may be generated. However, larger number of elements also increases required time to solve the problem. In this article, the term of mesh size is used to describe the inplane meshing, while number of layers is used to describe number of solid elements or shell sections through thickness. Accuracy of the buckling analysis in ANSYS is examined here for various values of mesh size, number of layers and various boundary conditions. Effects of inplane meshing and various boundary conditions on the linear eigenvalue buckling analysis in ANSYS is examined using shell models. Then effects of number of layers in the model is examined for functionally graded plates (FGP) using shell models, and for homogeneous plate using solid models with various element options.

5.1. Inplane mesh size

Shell models are implemented here to illustrate how inplane mesh size affects accuracy of buckling analysis in ANSYS for plates with various aspect ratios and thickness. Fig. 9 compares shell models of *Shell181* and *Shell281* elements, with various values of inplane mesh size, expressed as elements per plate edge, and various values of thickness, expressed as side-to-thickness ratio ranging from thin to moderately thick plates. Shell models used here are full models, i.e. with no symmetry expressed, as the one shown in Fig. 4-a. Plotted results are the error between buckling load obtained by ANSYS to those obtained using analytical solutions based on first-order shear-deformation theory (FSDT) as presented by Reddy [1], with a transverse shear-correction factor of 0.8925.

Results show that using smaller mesh size, i.e. larger number of elements per edge, gives higher accuracy solutions for different side-to-thickness ratios b/h. However, gain in solution accuracy reduces, as mesh size gets smaller. As seen in Fig. 9 for *Shell181* model, for each side-to-thickness ratio, mesh size of 80 and 100 elements per edge provide almost the same solution; furthermore, 40 and 100 elements per edge have no significant difference in their solutions. Accuracy of *Shell181* models seems to be more sensitive to the meshing size than the *Shell281* models. Models of *Shell281* provide solutions that are more accurate and closer to each other for various values of mesh size.

Another way to express mesh size is as element length that is independent of dimensions of the plate's edge. Fig. 10 shows solution accuracy of buckling analysis using *Shell181* and *Shell281* models of plate for various aspect ratios, i.e. plate's length-to-width ratio a/b, with a fixed element length. Accuracy is expressed as percentage error between ANSYS solutions and FSDT solutions. By using the same element length, larger plates, i.e. wider and/or longer, will contain more elements, which leads to results that are more accurate. Solution accuracy increases with increased number of elements, but at some point, it stops getting significantly better.

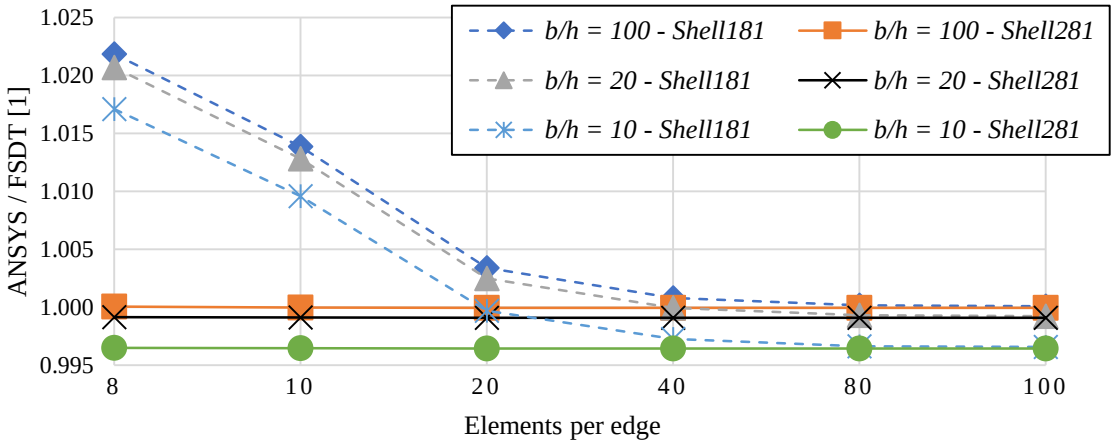

Fig. 9. ANSYS buckling solutions using shell models compared to FSDT [1] for various inplane mesh sizes and thickness values

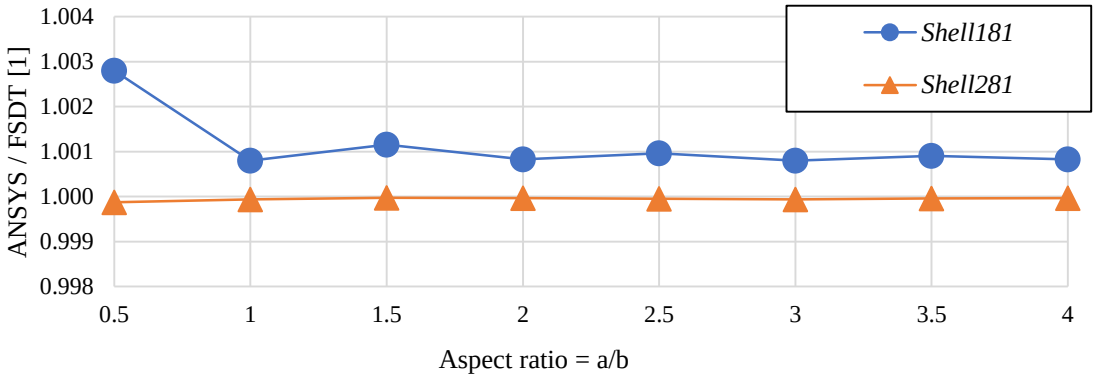

Fig. 10. ANSYS buckling solutions using shell models compared to FSDT [1] for various aspect ratios with fixed element length

The oscillation of solutions quality reflects the effect of the plate's aspect ratio. As a conclusion, even with the existence of variation in accuracy due to thickness of the plate, aspect ratio and mesh size, buckling loads calculated using both *Shell181* and *Shell281* models are very close to the FSDT solutions, while *Shell281* is more accurate and less sensitive to aspect ratio and number of elements.

5.2. Number of layers in shell model (FGP application)

Functionally graded materials (FGMs) are advanced inhomogeneous composite materials in which graded interlayer separates different materials of the composite structure [26, 27]. FGM's concept is to replace the sudden change in structure that occurs at the interface between different materials, with a compositionally graded phase, aiming at reducing stress concentrations through the structure [26]. This microstructure variation in FGM occurs with a specific function through one or more dimensions of the volume. Modeling the properties variation through one or more dimensions of functionally graded plate (FGP) in ANSYS could be accomplished using many methods. For instance, one method is using dummy thermal loads [28]. However, when the FGP has its properties variation only through its thickness, it becomes more convenient to stack layers with desired properties to present the FGP.

For shell models, number of layers means number of defined sections through thickness. ANSYS provides SECDATA command to define those sections and the relative thickness, material and orientation of each. Effect of number of layers on accuracy of shell model for buckling analysis is presented here. For shell model of homogeneous plate, number of layers does not alter the results. Therefore, to illustrate their effect on shell model accuracy, a composite plate is needed. A plate of functionally graded material (FGP) is modeled using shell elements and examined here.

Modeled FGP is a ceramic-metal composite plate, with elasticity modulus E varying linearly through its thickness and constant Poisson's ratio. Elasticity modulus of ceramic assumed as E_c= 380 GPa, for the metal as E_m= 70 GPa and Poisson's ratio as ν = 0.3. Aspect ratio a/b is taken as 0.5. Results are compared to solutions based on third-order deformation theory (TSDT) presented in the work of Shariat [29].

Fig. 11 shows the buckling load obtained by ANSYS for FGP shell model of *Shell281* elements compared to TSDT solutions, for various number of layers. Side-to-thickness ratio b/h is taken as 10. Results show that using small number of layers results in under-estimated buckling load. At the range of low number of layers, increasing the number of layers has significant effect on

the calculated buckling load, but at some point, change in results due change in number of layers starts to vanish. Although, it is often desired to have as many layers as possible to simulate the continuous variation in FGPs, models with very large number of layers consume long time in analysis, while not providing significantly different solutions than those with reasonably lower number of layers. For example, in the case shown in Fig. 11, model with 60 layers provides solution that is just slightly lower than the solution of model with 180 layers. Therefore, number of layers should be selected wisely to obtain accurate enough results with reasonable analysis time.

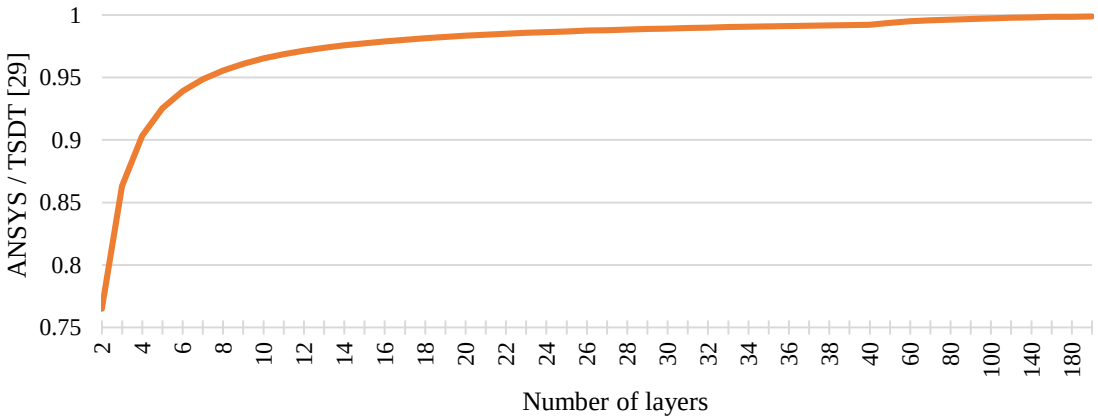

Fig. 11. ANSYS buckling solutions of FGP model of layered shell element compared to TSDT [29] for various number of layers

5.3. Options of shell elements

ANSYS provides options for elements to be tweaked in order to obtain better models for various applications. Among shell elements, *Shell181* has two interesting options to set. The first is the full integration option (KEYOPT(3) = 1), and the second is the advanced curve formulation option (KEYOPT(5) = 1). Effects of these options on the accuracy of buckling analysis are shown in Fig. 12. Shown analyses are conducted using the same plate model with the same element length. Therefore, reduced accuracy with increased aspect ratio is expected. It is observed that enabling option of full integration and/or advanced curve formulation slightly reduces the solution accuracy. However, both options reveal solutions those are very close to each other.

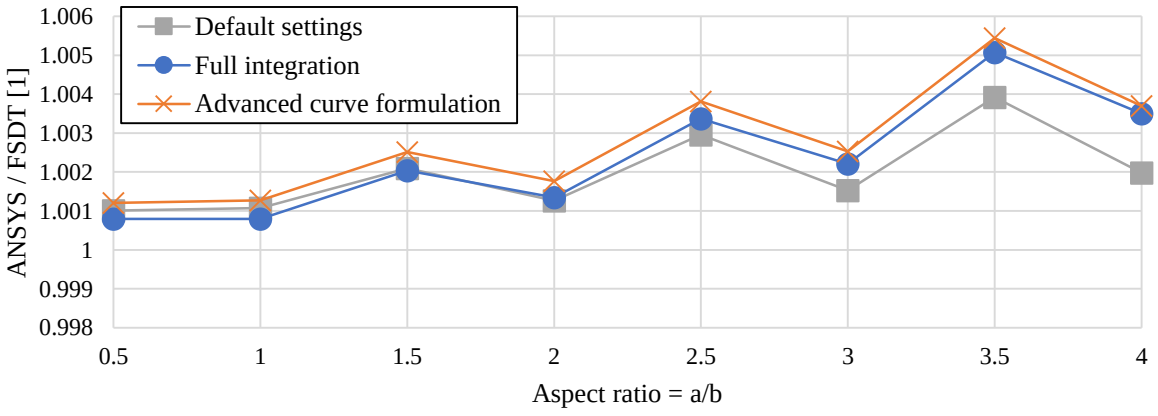

Fig. 12. ANSYS buckling solutions using *Shell181* model compared with FSDT [1] for various options of element technology and aspect ratios

5.4. Number of layers in solid model

Plates can be modeled as three-dimensional body using solid or solid-shell elements. In solid models, in addition to the inplane meshing one has to set the out-of-plane meshing even for homogeneous plates. Meshing through the thickness of the plate is expressed as number of layers. This section examines the effect of number of layers in solid model of a fully simply supported square plate (a = b = 1m) under uniaxial pressure for the same fine inplane element size and various values of plate's side-to-thickness ratios. ANSYS solutions obtained using various solid elements are compared to those obtained using FSDT theory presented by Reddy [1]. In addition, various elements' options are examined. Solid models used in the following analyses are symmetry models, as the one shown in Fig. 4-b.

5.4.1 Tetrahedral solid elements

Because of their shape, number of layers could not be set directly. Instead, plate is created by gluing as many thinner meshed plates as the demanded number of layers. Gluing operation in ANSYS is done using VGLUE [15] command. Steps of modeling plate as glued volumes are shown in Fig. 13. Each of these thinner plates can be assigned with different material properties in order to model composite plate. The case of homogeneous plate modeled with glued multi-layers is studied below.

Solutions of linear eigenvalue buckling analysis of plate modeled using tetrahedral solid elements compared to FSDT solutions are shown in Fig. 14-(a and b) for various number of layers and side-to-thickness ratios. Results show that plate model of *Solid187* elements seems to provide same solutions regardless of number of the layers. The other tetrahedral element *Solid285* does not provide right results for buckling analysis for small number of the layers, while being impractical to conduct the analysis with larger number of layers due to the long time consumption. It has been noted that it is really time consuming to analyze plate models of tetrahedral solid elements. No relevant options are available for these elements.

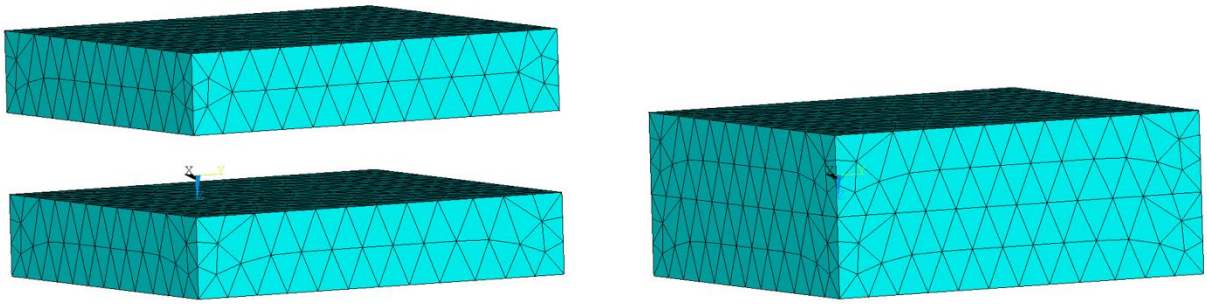

a) Step-1: Standalone meshed plates b) Step-2: Glued plates

Fig. 13. Multilayer glued plate modeling

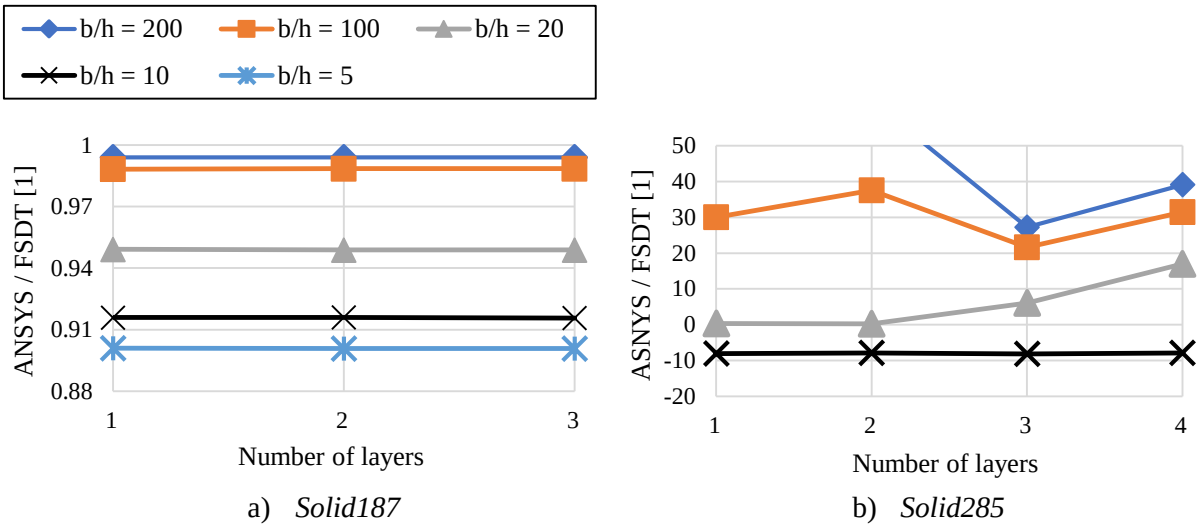

a) *Solid187* b) *Solid285*

Fig. 14. ANSYS buckling solutions using tetrahedral solid elements compared to FSDT [1] for various number of layers

5.4.2 Brick solid elements

With brick solid elements, number of layers through thickness can be modeled directly by setting the mesh size of the out-of-plane edges as demanded number of layers. Although not needed, gluing many meshed plates together is also a possible way to model multilayer plate with brick solid elements. A third way to model multilayered plate using these elements is by using the SECDATA command of ANSYS, which allows specifying thickness and material for layers through thickness. Relevant options of brick solid elements are examined for the linear eigenvalue analysis, and solutions compared to FSDT solutions are shown in Fig. 15 for *Solid185* and Fig. 16 for *Solid186* elements. For these analyses, plates are modeled as glued many single-layered plates. Results in Fig. 15 show that plate model of elements *Solid185*, has to have element technology option set as enhanced strain formulation or simplified enhanced strain formulation (KEYOPT (2) = 2 or 3). Other options for element technology include full integration with B method (KEYOPT (2) = 0), provides wrong results as shown in Fig. 15-b; and uniform reduced integration (KEYOPT (2) = 1), provides unstable results as shown in Fig. 15-c. Stable solution here means that solution does not significantly change anymore by increasing the number of layers.

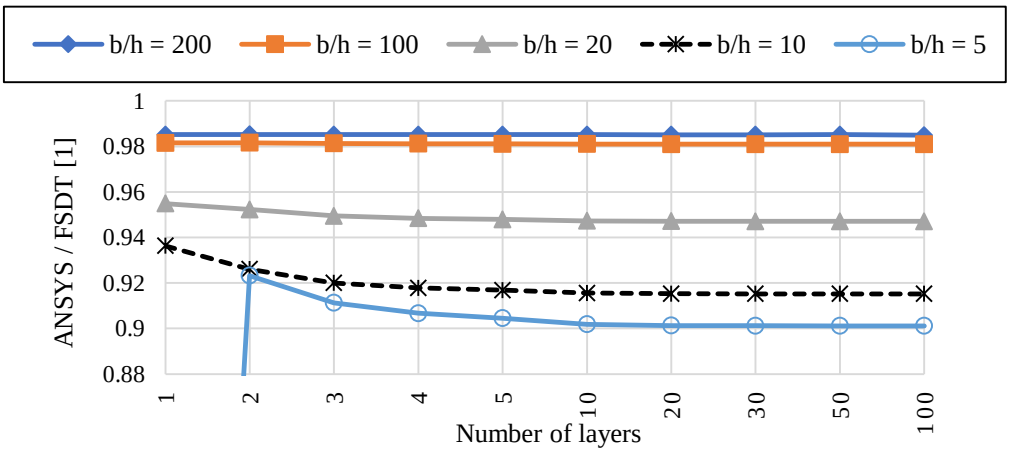

a) *Solid185*, KEYOPT(2) = 2 or KEYOPT(2) = 3

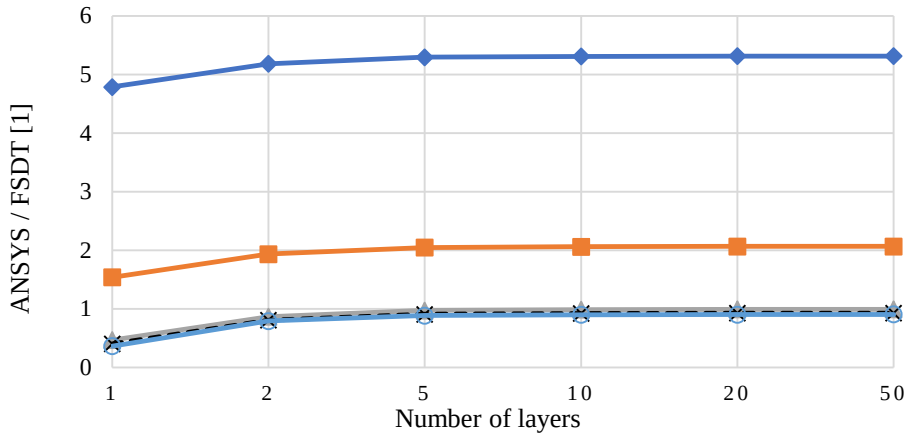

b) *Solid185*, KEYOPT(2) = 0

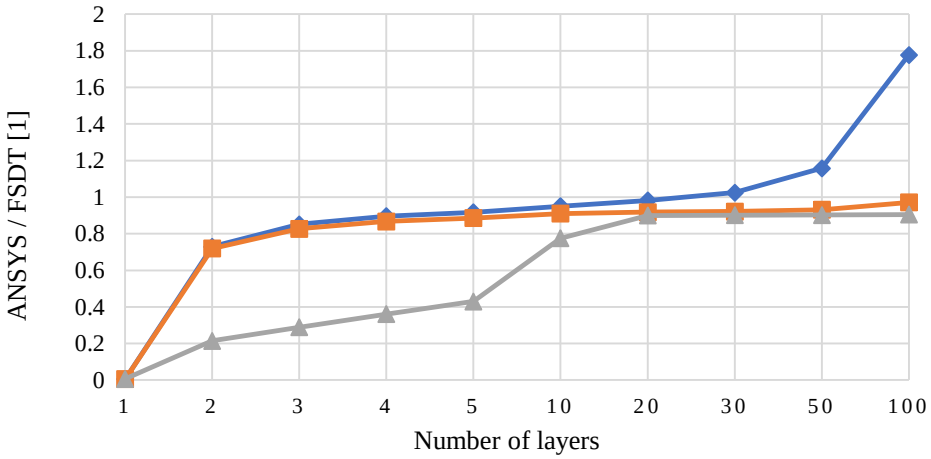

c) *Solid185*, KEYOPT(2) = 1

Fig. 15. ANSYS buckling solutions using *Solid185* elements compared with FSDT [1] for various options of element technology

The second brick solid element is *Solid186*. It has just two options for element technology to select one of them. The first option is the uniform reduced integration (KEYOPT (2) = 0) and the second is the full integration (KEYOPT (2) = 1). Both options provide stable solutions for any number of layers exceeds one. Results of buckling loads calculated by ANSYS for plate modeled by *Solid186* elements compared to FSDT solutions for both options are shown in Fig. 16-(a and b).

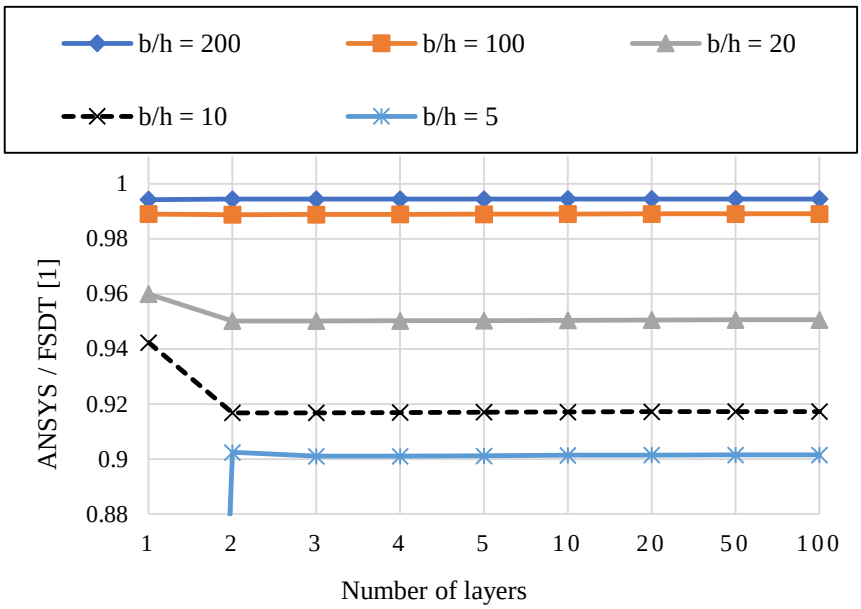

a) Solid186, KEYOPT(2) = 0

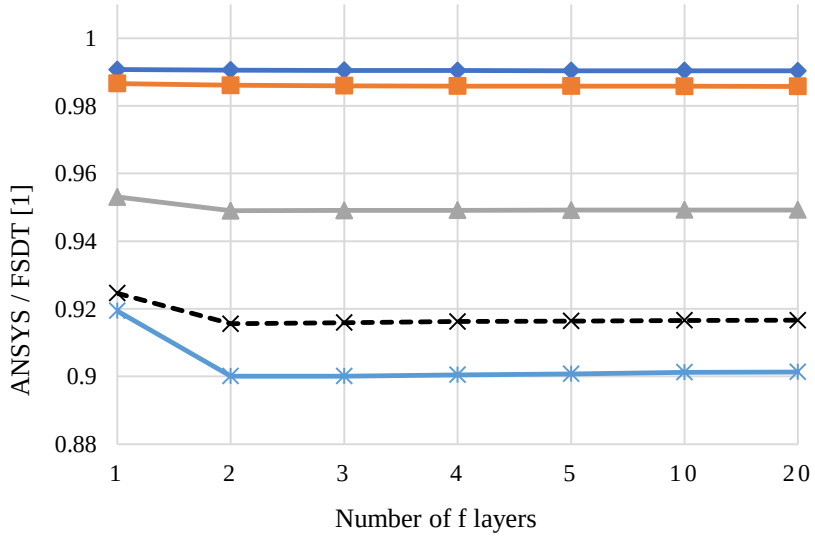

b) Solid186, KEYOPT(2) = 1

Fig. 16. ANSYS buckling analysis using *Solid186* elements compared to FSDT [1] for various options of element technology

5.4.3 Solid-shell element

Solid-shell element *Solsh190* is an advanced brick solid element with capabilities to simulate shells more accurately than solid elements. As shown in

Fig. 17, *Solsh190* provides better solutions for buckling analysis of thin plates than all other solid elements. Better solutions here means ANSYS solutions closer to FSDT. Here also, plates are modeled as glued thinner plates. It seems that *Solsh190* does not provide a stable solution even for large number of layers. Solutions do not stop decreasing as number of layers increases.

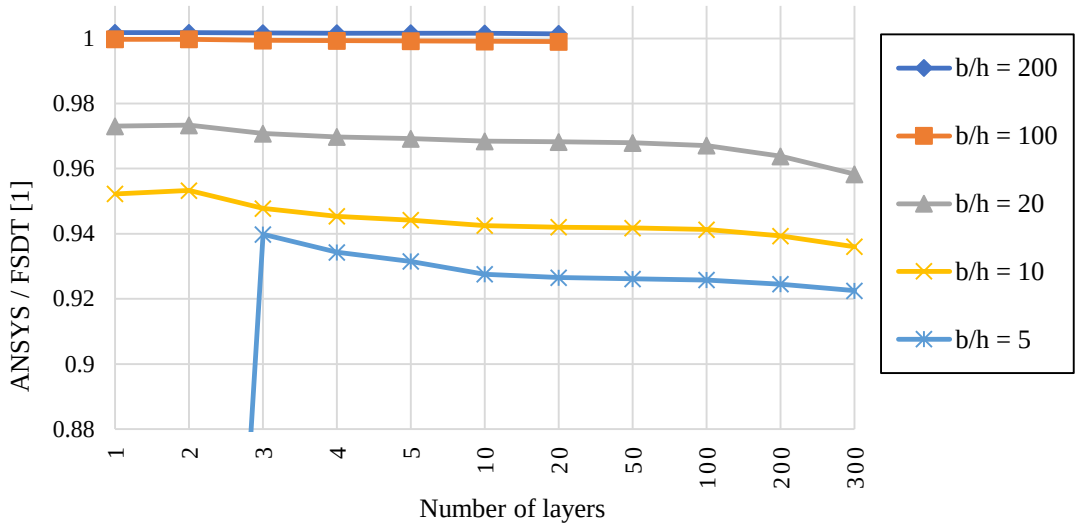

Fig. 17. ANSYS buckling analysis using *Solsh190* elements compared to FSDT [1] for various number of layers

Results of using solid models with various number of layers shows that models of solid elements (*Solid185*, *Solid186* and *Solid187*) and solid-shell element (*Solsh190*) start to provide stable solutions when enough number of layers and suitable settings are provided. Required number of layers depends on thickness of plate and the elements type used in the model. Thin plates may require just one layer, while thicker plates require more to provide stable solutions. For lower number of layers, plate behaves stiffer, i.e. ANSYS over-predicts the buckling load. For very thick plates, when very low number of layers is used, wrong under-estimated buckling loads result. Even though model of *Solid187* elements seems to give stable solutions even when just a single layer is in use, this model is very time consuming in analysis compared with other solid models. For thick plates, solid model of solid-shell element *Solsh190* tends to further under-estimate the buckling load with increased number of layers. Using large number of layers with thin plates may cause the analysis to crash or consume long time to end. As shown in

Fig. 17, starting from 20 layers, thin plates of b/h $\leq$ 100 cause the analysis to crash and no solution is revealed. Therefore, one have to select number of layers wisely to be in the range that provides accurate results and at the same time does not crash or consume much time. Number of layers to be selected is the number that if increased no significant gain in accuracy is actually obtained.

6. Boundary conditions effect

To examine behavior of the plate model with various boundary conditions, shell models of plate under various boundary conditions are analyzed in ANSYS. Thin plates with side-to-thickness ratio (b/h) of 200 are considered, so that plate be comparable to the available analytical solutions based on the classical plate theory (CPT) which presented by Reddy [1]. CPT normally over-estimates the buckling load, so it is expected to obtain buckling loads from ANSYS having lower values than those of CPT.

Fig. 18-(a, b and c) show results for various boundary conditions and various aspect ratios.

Fig. 18-a shows results for plates simply supported at two opposite edges while clamped at the other two edges.

Fig. 18-b shows results for the plates but with one of the clamped edges being free.

Fig. 18-(c and d) show the first and second buckling loads for a plate that is simply supported at three edges while the last is free. In all these analyses, *Shell281* models predicts buckling loads lower than those predicted by *Shell181* models; and has narrower variation in term of solution accuracy. In addition, it is noticed that both shell models are accurate in predicting buckling load for plates, given that plate is meshed into enough number of elements. That is correct for also higher buckling modes, as shown in

Fig. 18-d, the second buckling load obtained and compared to CPT results; and same behavior and high accuracy observed.

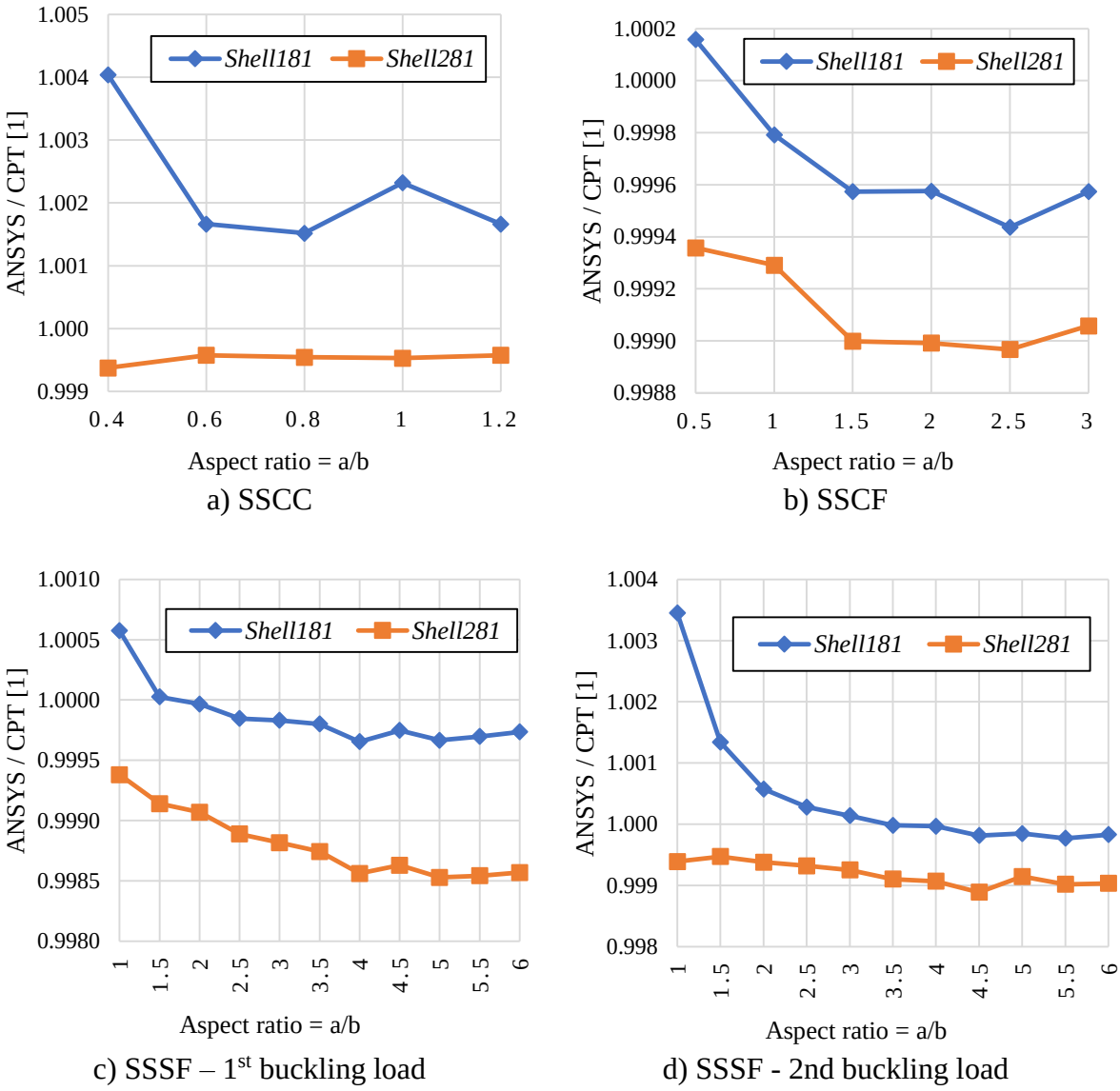

Fig. 18. ANSYS buckling analysis using shell models compared to CPT [1] for various boundary conditions and aspect ratios

7. Choosing plate model

Shell and solid plate models in ANSYS provide different solutions for buckling analysis. Choosing a model for plate buckling analysis in ANSYS depends on the thickness. Shell models provide results that are more accurate for thinner plates, while solid models provide results that are more accurate for thicker ones. However, solid models of solid-shell elements seem to be more accurate than other solid models for both thin and thick plates. Fig. 19 compares between stable results of non-dimensional linear eigenvalue buckling load for various solid and shell models of a square plate under uniform uniaxial pressure, along with solutions based on 3D elasticity theory, FSDT and CPT for plates ranging from thin to thick plates. The 3D elasticity solution is taken from Moslemi [30]. Non-dimensional buckling load ($\bar{N}_{cr}$) is calculated as:

$$\bar{N}_{cr} = N_{cr}\frac{b^2}{\pi^2 D}$$

N_{cr} = buckling load in (N/mm), b = side length of the plate, D is the flexural rigidity, calculated as:

$$D = h^3\frac{E}{12(1-\nu^2)}$$

h = thickness of the plate, E and ν are elasticity modulus and Poisson's ratio of the material of the plate. Solid models of solid elements provide almost the same results for thick plates but different results for thin plates, while solid model of solid-shell element provides a more consistent with solutions based on 3D elasticity theory for thicker plates, and with FSDT for thinner ones.

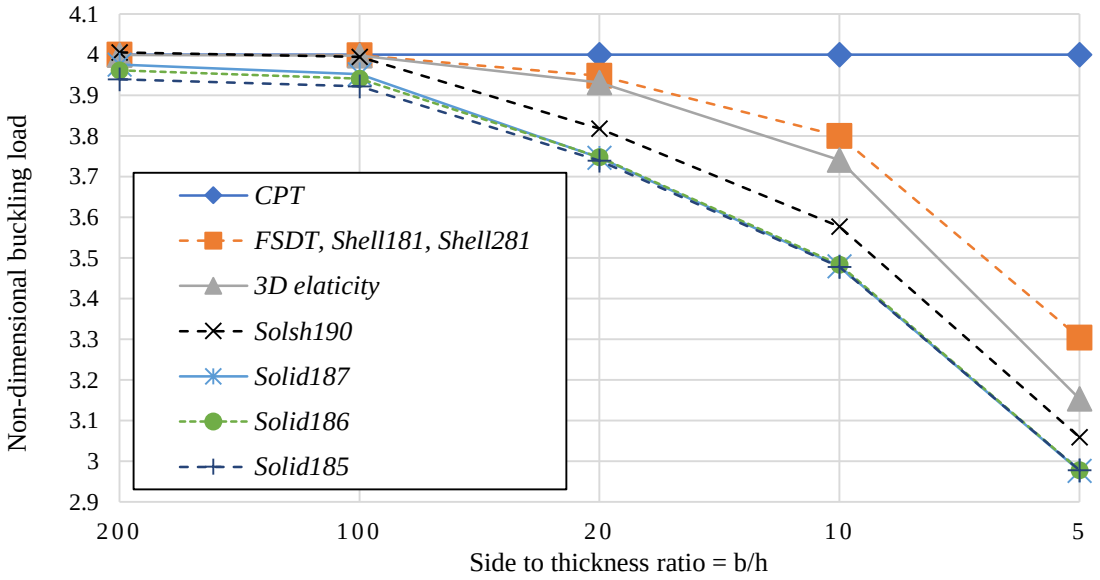

Fig. 19. ANSYS buckling analysis using solid models compared with solutions based on 3D elasticity [30], FSDT [1] and CPT [1] for square plate under uniaxial pressure.

Fig. 20 shows another comparison of linear eigenvalue buckling loads obtained by ANSYS using various solid models along with solutions based on CPT, FSDT and 3D elasticity theory, a square plate under uniform equal biaxial compression. Generally, solid models behave similar to their behavior in the uniaxial case, Fig. 19. Again, models of *Solsh190* are the most consistent

with FSDT for thin plates, and with 3D elasticity solution for thicker plates. Models of solid elements provide similar results for thick plates, but different results for thinner plates, which have significant discrepancy from FSDT, compared to the *Solsh190* element. As a conclusion, for thin plates shell models, specifically *Shell281*, should be used, while for thicker plates solid models of *Solsh190* are more accurate.

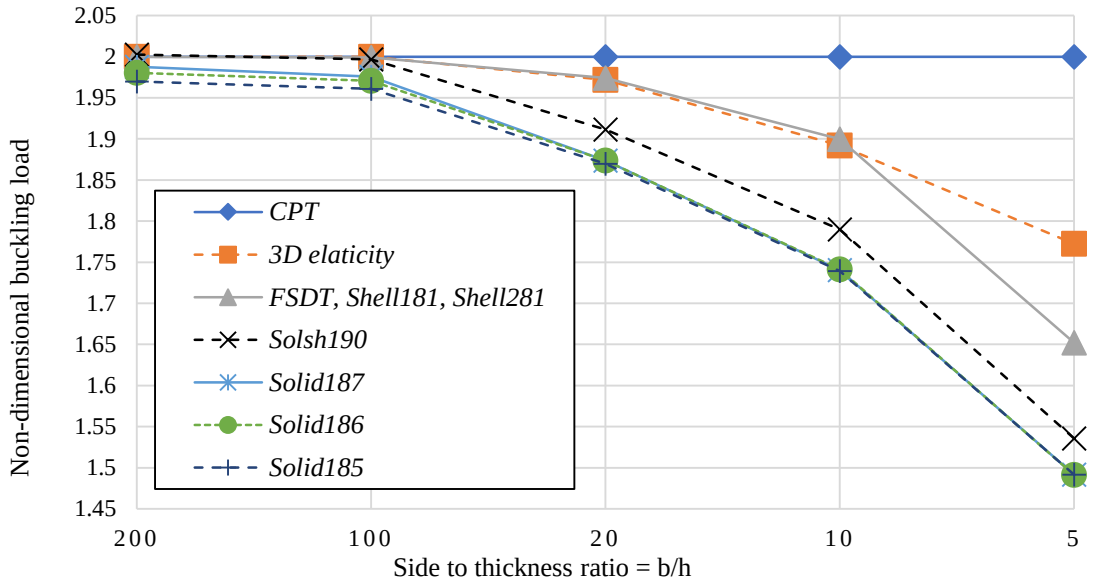

Fig. 20. ANSYS buckling analysis using solid models compared with solutions based on 3D elasticity [30], FSDT [1] and CPT [1] for square plate under equal-biaxial pressure

8. Conclusion

Rectangular plate buckling in ANSYS has been presented through comparative studies. Modeling both isotropic and functionally graded rectangular plates, various boundary conditions and meshing of plate structure in ANSYS have been discussed. Various buckling analysis procedures are also discussed. Results obtained from ANSYS are compared with analytical solutions based on various plate theories and 3D elasticity theory.

Meshing plays an important role in obtaining accurate results. Just enough number of elements is needed; much more elements lead to slower analysis with no significant gain in accuracy, while very low number of elements leads to wrong solutions. It is found that selecting plate model depends on the plate thickness. Comparisons in this study show that shell models of rectangular plate have the highest accuracy for thin plates. Models of *Shell281* elements are less sensitive to mesh density and it is more accurate compared to the model with *Shell181* elements.

Not all solid elements are appropriate for plate buckling analysis; *Solid285* provides wrong solutions even with high number of elements. *Solid185* has to be implemented with cautious, because for some sets of options it does not provide right solutions. Solid models of appropriate solid elements under-estimate the buckling load for thin plates with different error for each model, while they have the same solutions for thick plates. Solid model of solid-shell elements has accurate solutions close to shell models solutions for thin plates, but for thick plates, its solutions are higher than other solid models, while being significantly lower than shell models and closer to the solutions those based on 3D elasticity theory.

Because of the wide range of element types and options in ANSYS, having this comparative study facilitates using the software more efficiently in performing buckling analyses on rectangular plates. Future works may include conducting the same comparative study on buckling of plates but with other geometries, e.g. circular, annual, skew and perforated. In addition, buckling of composite plates including functionally graded plates may be investigated more thoroughly in future works, along with thermal and thermo-mechanical buckling analyses.

References

[1] J. N. Reddy, Theory and analysis of elastic plates and shells, CRC press, 2nd Edition, 2006.

[2] M. R. Eslami, Eslami, and Jacobs, Buckling and Postbuckling of Beams, Plates, and Shells, Springer, 2018.

[3] R. M. Jones, Buckling of bars, plates, and shells, Bull Ridge Corporation, 2006.

[4] K. Bhaskar and T. Varadan, Plates: theories and applications, John Wiley & Sons, 2014.

[5] C. H. Yoo and S. Lee, Stability of structures: principles and applications, Elsevier, 2011.

[6] K. Mercan; and Ö. Civalek, Modal Analysis of Micro and Nanowires Using Finite Element Softwares, *International Journal Of Engineering & Applied Sciences,* 10(4), 291 - 304, 2019.

[7] B. Banerjee, J. Chen, and A. Kathirgamanathan, Comparison of ANSYS elements SHELL181 and SOLSH190, *Res. Rep., Univ. of Auckland, New Zealand,* 2011.

[8] E. Wang, "Thin-wall structure simulation," presented at the 2006 International ANSYS Conference, 2006.

[9] M. S. Swamy, R. A, S. D, and S. S. Badami, Buckling Analysis of Plate Element Subjected to In Plane Loading Using ANSYS, *International Journal of Innovative Research in Science, Engineering and Technology*, 4(5), 10, 2015.

[10] T. Subramani and A. Sugathan, Finite element analysis of thin walled-shell structures by ANSYS and LS-DYNA, *International Journal of Modern Engineering Research,* 2(4), 1576-1587, 2012.

[11] M. Bischoff, "Modeling of shells with three-dimensional finite elements," in *Proceedings of the 6th International Conference on Computation of Shell and Spatial Structures. May,* 28-31, 2008.

[12] "Introducing APDL," in *ANSYS® Release 17.1, Help System, Mechanical APDL, ANSYS Parametric Design Language Guide*: ANSYS, Inc.

[13] "SHELL181," in *ANSYS® Release 17.1, Help System, Mechanical APDL, Element Reference, Element Library*: ANSYS, Inc.

[14] "SHELL281," in *ANSYS® Release 17.1, Help System, Mechanical APDL, Element Reference, Element Library*: ANSYS, Inc.

[15] "Performing a Nonlinear Buckling Analysis," in *ANSYS® Release 17.1, Help System, Mechanical APDL, Structural Analysis Guide, Buckling Analysis*: ANSYS, Inc.

[16] "Command Reference," in *ANSYS® Release 17.1, Help System, Mechanical APDL*: ANSYS, Inc.

[17] "SOLID285," in *ANSYS® Release 17.1, Help System, Mechanical APDL, Element Reference, Element Library*: ANSYS, Inc.

[18] "SOLID187," in *ANSYS® Release 17.1, Help System, Mechanical APDL, Element Reference, Element Library*: ANSYS, Inc.

[19] "SOLID185," in *ANSYS® Release 17.1, Help System, Mechanical APDL, Element Reference, Element Library*: ANSYS, Inc.

[20] "SOLID186," in *ANSYS® Release 17.1, Help System, Mechanical APDL, Element Reference, Element Library*: ANSYS, Inc.

[21] "Types of Buckling Analyses," in *ANSYS® Release 17.1, Help System, Mechanical APDL, Structural Analysis Guide, Buckling Analysis*: ANSYS, Inc.

[22] "SOLSH190," in *ANSYS® Release 17.1, Help System, Mechanical APDL, Element Reference, Element Library*: ANSYS, Inc.

[23] "Nonlinear Buckling Analysis," in *ANSYS® Release 17.1, Help System, Mechanical Applications, Mechanical User's Guide, Analysis Types, Linear Dynamic Analysis Types*: ANSYS, Inc.

[24] "Procedure for Eigenvalue Buckling Analysis," in *ANSYS® Release 17.1, Help System, Mechanical APDL, Structural Analysis Guide, Buckling Analysis*: ANSYS, Inc.

[25] "Eigenvalue Buckling Analysis," in *ANSYS® Release 17.1, Help System, Mechanical Applications, Mechanical User's Guide, Analysis Types, Linear Dynamic Analysis Types*: ANSYS, Inc.

[26] Y. Miyamoto, W. Kaysser, B. Rabin, A. Kawasaki, and R. G. Ford, Functionally graded materials: design, processing and applications, Springer Science & Business Media, 1999.

[27] V. Birman, T. Keil, and S. Hosder, "Functionally graded materials in engineering," in *Structural Interfaces and Attachments in Biology*, vol. 9781461433170: Springer New York, 19-41,2013.

[28] A. H. A. Hassan and İ. Keleş, FGM Modelling using Dummy Thermal Loads, *Journal of Selcuk International Science and Technology*, 1(10-16), 2017.

[29] B. S. Shariat and M. Eslami, Buckling of thick functionally graded plates under mechanical and thermal loads, *Composite Structures*, 78(3), 433-439, 2007.

[30] A. Moslemi, B. N. Neya, and J. V. Amiri, 3-D elasticity buckling solution for simply supported thick rectangular plates using displacement potential functions, *Applied Mathematical Modelling*, 40(11-12), 5717-5730, 2016.

International Journal of Engineering & Applied Sciences (IJEAS)
Vol.11, Issue 1 (2019) 330-344
http://dx.doi.org/10.24107/ijeas.533727
Int J Eng Appl Sci 11(1) (2019) 330-344

Buckling Analysis of Steel Fiber Column with Different Cross-Section and Boundary Conditions Using Euler-Bernoulli Beam Theory

M. Tunahan Özdemir [a], Veysel Kobya [b], Mustafa Özgür Yaylı [c], Ali Mardani-Aghabaglou [d]

[a,b,c,d] *Faculty of Engineering, Civil Engineering Departmant, Uludag University, Bursa, Turkey*
E-mail adress: 501726009@ogr.uludag.edu.tr [a], 511826008@ogr.uludag.edu.tr [b],
ozguryayli@uludag.edu.tr [c], alimardani@uludag.edu.tr [d]

ORCİD numbers of authors
0000-0001-9313-9666 [a], 0000-0002-1226-8405 [b], 0000-0003-2231-170X [c], 0000-0003-0326-5015 [d]

Received date: 22.02.2019
Accepted date: 09.04.2019

Abstract

Nowadays, with the help of developing technology, engineering problems which are difficult to solve have become easily solved in a short time by means of computer software. Certain mathematical algorithms are used in these analysis methods. The mathematical and numerical solution methods created provide a significant solution facility for engineering. In this paper, the buckling analysis of the Euler column model, with elastic boundaries and containing steel fibers, under pressure effect is performed. In the column model, three different sections, which have been produced from four different concrete series, including three different types of fiber reinforced specimens and one non-fibrous control sample(C) with 0.6% by volume, were analyzed by using a software. In the study, the analysis of the critical buckling values depends on length, elastic modulus and cross-sectional type of the column model has been performed. The results are shown in graphs and tables. With the results of the analysis, the effect of slenderness and steel fiber concrete on the critical load in pressure columns have been investigated.

Keywords: Elastically restrained ends, Euler columns, steel fiber reinforcement, comparison of buckling load

1. Introduction

Nowadays, with the developing technology, the results obtained from the engineering point of view are closer to reality. Analysis that are difficult to calculate are solved in a much shorter time with the help of computers and thus, it becomes easier to obtain different solution methods. In the light of these developments, various approaches have been presented to investigate the buckling behavior of structural elements under axial load. Due to various modelling, design and analysis difficulties with the finite element method, which is a method used for analyzing buckling behavior of structural elements in civil engineering, it is needed to use computer programs. At the beginning of the modelling and analysis process, Euler said that the pressure columns have been not only crushed but they also have stability problems [1]. Euler pioneered the researchers in analytical analysis of elastic columns and since the first study has been carried out in this area in 1744, the analysis has been called Euler load [2]. After Euler's first step for stability analysis, many researchers have contributed to the modelling of structural elements closer to reality. A.N. Dinnik [3] has designed the variable cross-section type of the column and

beam elements, which is pinned from one end, clamped on the other end. And he examined the buckling behavior of them.
J.B. Keller [4] has studied the mechanical behavior of the circular cross-section and equilateral triangular section column and obtained results for the nonlinear buckling problem. Mechanical behaviors for similar Euler columns have been examined by I. Tadjbakhsh & J.B. Keller, [5] and J.E. Taylor, [6], and exact results have been obtained for different boundary conditions. S. Timoshenko [7] has contributed to the realistic results by adding slip and rotational momentum factors in the beam to the Euler-Bernoulli theory Lee et al. [8-11] on the buckling loads, have made studies suitable for use in design. Q. Li, H. Cao, & G. Li, [12], L. Qiusheng, C. Hong & L. Guiqing [13] and Q. Li, H. Cao, & G. Li, [14], in their work, using Bessel functions and super geometric functions, gave the flexural formulation of elastic columns with variable cross-section. He has stated that the axial load and bending stiffness distribution of the high structures are appropriately described. Kim and Kim [15] have presented a method of calculating the vibration frequency of beams in boundary conditions created by using the Fourier series, which is generally restrained and non-classical limiting methods of rotation and cycle springs.

M.T. Atay & S.B. Coşkun [16], S.B. Coşkun & M.T. Atay [17] have formed a column model with variable section and an elastically constrained along the upper and lower end and performed stability analysis with the Variational Iteration Method (VIM). K.V. Singh & G. Li [18] in their study, they have created mathematical modelling of the Transcendental Eigenvalue Problem (TOE) using the previously proposed NEIM (numerical algorithm) numerical algorithm of axially graded and elastically constrained columns. He has performed a buckling analysis. The researchers has used many analytical and numerical methods to model column and beam elements and compared their results with experimental results or to each other [19-33], similar to the approaches used in the column elements have been also studied in the beam elements [34-41].

Gül and Aydoğlu [42], in their study, beams on elastic foundation have examined in terms of the wave number vibrations with Euler-Bernoulli and Timoshenko beam theories using Hamilton’s Principle. In the study by Y. Zhang et al. [43], using the kp-Ritz method for numerical solutions in buckling analysis, have been investigated the graphene layers in which the elastic medium has been modelled by the Winkler method. M.Ö. Yaylı [44] modelled the Euler column, which is bounded along its length and had different boundary conditions at its end points. In this numerical modelling, Stokes' transformations and Furier series have been used to create the coefficients matrix.

In this study, column model which is investigated by M.Ö. Yaylı [44] has been created by using Euler's column theory. Firstly, the equation of the well-known Euler-Bernoulli beam theory in the literature is given under axial loads. Fourier sine series of displacement function is chosen to obtain analytical general solutions by M.Ö. Yaylı [44]. Elasticity modules for Euler-Bernoulli column type structural elements with an external load applied at the upper and lower ends of the column with different boundary conditions have been calculated experimentally. In three different column sections produced from four different concrete series as, F30, F35, F50 fiber reinforced concrete and non-fibrous (C) sample, buckling analysis by using Mathematica program is made by taking the weight of the column element into account.

2. Numerical Modelling of the Column to be Analyzed

Fig. 1 shows the Euler column model which is elastically limited along the length of the column and has different boundary conditions. Government equation for buckling Timoshenko and Gere [45] and Wang et al. [46]:

$$\frac{d^2}{dx^2}\left[EI\frac{d^2y}{dx^2}\right] + P\frac{d^2y}{dx^2} + k_w y = 0 \quad (1)$$

In the equation, EI is the bending stiffness, P is the axial load applied from the column end points, k_w is the elastic limitation coefficient known as Winklers' constant applied for each unit length along the column length. M.Ö. Yaylı [44] in his study, obtained a matrix of coefficients representing the column model with a study of Stokes' transformations for the development of stability equations which limited the lateral displacements of the Furier sinus series. With this approach, it was stated that the buckling analysis of the Euler columns would yield closer results to the truth under different boundary conditions.

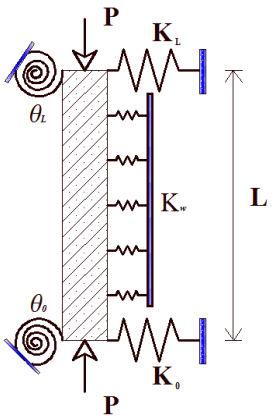

Fig. 1. An elastically restrained Euler column model.

Displacement function to apply Stokes' transformation:

$$y(x) = \begin{Bmatrix} \delta_0 & x = 0 \\ \delta_L & x = L \\ \sum_{n=1}^{\infty} C_n \sin\left[\frac{n\pi x}{L}\right] & 0 < x > L \end{Bmatrix} \quad (2)$$

The Stokes transform are obtained using the displacement function and the Fourier series by M.Ö. Yaylı [44];

$$y(x) = \sum_{n=1}^{\infty} \frac{2\alpha_n((-1)^n(\delta_L(P-EI\alpha_n{}^2)+EI\delta_L'')+\delta_0(EI\alpha_n{}^2-P)-EI\delta_0'')}{L(EI\alpha_n{}^4+k_w-P\alpha_n{}^2)} \sin\left(\frac{n\pi x}{L}\right) \quad (3)$$

Four homogeneous equations are obtained by applying the boundary [44]:

- Boundary conditions:

$$K_0\delta_0 = -EI\frac{d^3y(x)}{dx^3}, \quad x = 0 \quad (4)$$

$$K_L\delta_L = -EI\frac{d^3y(x)}{dx^3}, \quad x = L \quad (5)$$

$$\theta_0\frac{dy(x)}{dx} = EI\frac{d^2y(x)}{dx^2}, \quad x = 0 \quad (6)$$

$$\theta_L\frac{dy(x)}{dx} = -EI\frac{d^2y(x)}{dx^2}, \quad x = L \quad (7)$$

- Homogeneous equations:

$$(-\bar{K_0} - \sum_{n=1}^{\infty} \frac{2n^2\pi^2\bar{K_w}}{n^4\pi^4-\bar{P_b}n^2\pi^2+K_w}) \frac{\delta_0}{L^2} + (\sum_{n=1}^{\infty} \frac{2n^2(-1)^n\pi^2\bar{K_w}}{n^4\pi^4-\bar{P_b}n^2\pi^2+K_w}) \frac{\delta_L}{L^2} +$$

$$(1 + \sum_{n=1}^{\infty} \frac{2(\bar{K_w}-\bar{P_b}n^2\pi^2)}{n^4\pi^4-\bar{P_b}n^2\pi^2+K_w})\delta_0{}'' + (1 + \sum_{n=1}^{\infty} \frac{2(-1)^n(\bar{K_w}-\bar{P_b}n^2\pi^2)}{n^4\pi^4-\bar{P_b}n^2\pi^2+K_w})\delta_L{}'' = 0 \quad (8)$$

$$(\sum_{n=1}^{\infty} \frac{2n^2(-1)^n\pi^2\bar{K_w}}{n^4\pi^4-\bar{P_b}n^2\pi^2+K_w}) \frac{\delta_0}{L^2} + (-\bar{K_L} - \sum_{n=1}^{\infty} \frac{2n^2\pi^2\bar{K_w}}{n^4\pi^4-\bar{P_b}n^2\pi^2+K_w}) \frac{\delta_L}{L^2}$$

$$+ (1 + \sum_{n=1}^{\infty} \frac{2(-1)^n(\bar{K_w}-\bar{P_b}n^2\pi^2)}{n^4\pi^4-\bar{P_b}n^2\pi^2+K_w})\delta_0{}'' + (1 + \sum_{n=1}^{\infty} \frac{2(\bar{K_w}-\bar{P_b}n^2\pi^2)}{n^4\pi^4-\bar{P_b}n^2\pi^2+K_w})\delta_L{}'' = 0 \quad (9)$$

$$-(\bar{\theta_0} + 2\bar{\theta_0} \sum_{n=1}^{\infty} \frac{\bar{K_w}}{n^4\pi^4-\bar{P_b}n^2\pi^2+K_w}) \frac{\delta_0}{L^2} + (\bar{\theta_0} + 2\bar{\theta_0} \sum_{n=1}^{\infty} \frac{(-1)^n\bar{K_w}}{n^4\pi^4-\bar{P_b}n^2\pi^2+K_w}) \frac{\delta_L}{L^2}$$

$$+ (-1 - 2\bar{\theta_0} \sum_{n=1}^{\infty} \frac{n^2\pi^2}{n^4\pi^4-\bar{P_b}n^2\pi^2+K_w})\delta_0{}'' + (2\bar{\theta_0} \sum_{n=1}^{\infty} \frac{n^2\pi^2(-1)^n}{n^4\pi^4-\bar{P_b}n^2\pi^2+K_w})\delta_L{}'' = 0 \quad (10)$$

$$-(\bar{\theta_L} + 2\bar{\theta_L} \sum_{n=1}^{\infty} \frac{(-1)^n\bar{K_w}}{n^4\pi^4-\bar{P_b}n^2\pi^2+K_w}) \frac{\delta_0}{L^2} + (\bar{\theta_L} + 2\bar{\theta_L} \sum_{n=1}^{\infty} \frac{\bar{K_w}}{n^4\pi^4-\bar{P_b}n^2\pi^2+K_w}) \frac{\delta_L}{L^2} +$$

$$(2\bar{\theta_L} \sum_{n=1}^{\infty} \frac{n^2\pi^2(-1)^n}{n^4\pi^4-\bar{P_b}n^2\pi^2+K_w})\delta_0{}'' + (-1 - 2\bar{\theta_L} \sum_{n=1}^{\infty} \frac{n^2\pi^2}{n^4\pi^4-\bar{P_b}n^2\pi^2+K_w})\delta_L{}'' = 0 \quad (11)$$

Where

$$\bar{\theta_L} = \frac{\theta_L \mathrm{L}}{\mathrm{EI}},\ \bar{\theta_0} = \frac{\theta_0 \mathrm{L}}{\mathrm{EI}},\ \bar{K_0} = \frac{K_0 L^3}{\mathrm{EI}},\ \bar{K_L} = \frac{K_L L^3}{\mathrm{EI}},\ \bar{K_w} = \frac{k_w L^4}{\mathrm{EI}},\ \ \bar{P_b} = \frac{\mathrm{P}L^2}{\mathrm{EI}} \quad (12)$$

Equations are written in matrix form M.Ö. Yaylı [44]:

$$\begin{bmatrix} \psi_{11} & \psi_{12} & \psi_{13} & \psi_{14} \\ \psi_{21} & \psi_{22} & \psi_{23} & \psi_{24} \\ \psi_{31} & \psi_{32} & \psi_{33} & \psi_{34} \\ \psi_{41} & \psi_{42} & \psi_{43} & \psi_{44} \end{bmatrix} \begin{bmatrix} \frac{\delta_0}{L^2} \\ \frac{\delta_L}{L^2} \\ \delta_0{}'' \\ \delta_L{}'' \end{bmatrix} = 0 \quad (13)$$

The eigenvalue system gives the critical buckling load M.Ö. Yaylı [44].

$$\left|\psi_{ij}\right| = 0, \quad \text{(i,j = 1, 2, 3, 4)} \quad (14)$$

Where

$$\psi_{11} = -\bar{K_0} - \sum_{n=1}^{\infty} \frac{2n^2\pi^2\bar{K_w}}{n^4*\pi^4-\bar{P_b}*n^2*\pi^2+\bar{K_w}}, \qquad \psi_{12} = \sum_{n=1}^{\infty} \frac{2n^2(-1)^n\pi^2\bar{K_w}}{n^4*\pi^4-\bar{P_b}*n^2*\pi^2+\bar{K_w}} \quad (15)$$

$$\psi_{12} = 1 + \sum_{n=1}^{\infty} \frac{2(\bar{K_w}-\bar{P_b}n^2\pi^2)}{n^4*\pi^4-\bar{P_b}*n^2*\pi^2+\bar{K_w}}, \qquad \psi_{14} = 1 + \sum_{n=1}^{\infty} \frac{2(-1)^n(\bar{K_w}-\bar{P_b}n^2\pi^2)}{n^4*\pi^4-\bar{P_b}*n^2*\pi^2+\bar{K_w}} \quad (16)$$

$$\psi_{21}=\sum_{n=1}^{\infty}\frac{2n^2(-1)^n\bar{K_w}\pi^2}{n^4*\pi^4-\bar{P_b}*n^2*\pi^2+\bar{K_w}},\qquad \psi_{22}=-\bar{K_L}-\sum_{n=1}^{\infty}\frac{2n^2\bar{K_w}\pi^2}{n^4*\pi^4-\bar{P_b}*n^2*\pi^2+\bar{K_w}} \tag{17}$$

$$\psi_{23}=1+\sum_{n=1}^{\infty}\frac{2(-1)^n(\bar{K_w}-\bar{P_b}n^2\pi^2)}{n^4*\pi^4-\bar{P_b}*n^2*\pi^2+\bar{K_w}},\qquad \psi_{24}=1+\sum_{n=1}^{\infty}\frac{2(\bar{K_w}-\bar{P_b}n^2\pi^2)}{n^4*\pi^4-\bar{P_b}*n^2*\pi^2+\bar{K_w}} \tag{18}$$

$$\psi_{31}=\bar{\theta_0}+2\bar{\theta_0}\sum_{n=1}^{\infty}\frac{\bar{K_w}}{n^4*\pi^4-\bar{P_b}*n^2*\pi^2+\bar{K_w}},\qquad \psi_{32}=-\bar{\theta_0}+2\bar{\theta_0}\sum_{n=1}^{\infty}\frac{(-1)^n\bar{K_w}}{n^4*\pi^4-\bar{P_b}*n^2*\pi^2+\bar{K_w}} \tag{19}$$

$$\psi_{33}=-1-2\bar{\theta_0}\sum_{n=1}^{\infty}\frac{n^2\pi^2}{n^4*\pi^4-\bar{P_b}*n^2*\pi^2+\bar{K_w}},\qquad \psi_{34}=2\bar{\theta_0}\sum_{n=1}^{\infty}\frac{n^2\pi^2(-1)^n}{n^4*\pi^4-\bar{P_b}*n^2*\pi^2+\bar{K_w}} \tag{20}$$

$$\psi_{41}=-\bar{\theta_L}+2\bar{\theta_L}\sum_{n=1}^{\infty}\frac{(-1)^n\bar{K_w}}{n^4*\pi^4-\bar{P_b}*n^2*\pi^2+\bar{K_w}},\qquad \psi_{42}=\bar{\theta_L}+2\bar{\theta_L}\sum_{n=1}^{\infty}\frac{\bar{K_w}}{n^4*\pi^4-\bar{P_b}*n^2*\pi^2+\bar{K_w}} \tag{21}$$

$$\psi_{43}=2\bar{\theta_L}\sum_{n=1}^{\infty}\frac{n^2\pi^2(-1)^n}{n^4*\pi^4-\bar{P_b}*n^2*\pi^2+\bar{K_w}},\qquad \psi_{44}=-1-2\bar{\theta_L}\sum_{n=1}^{\infty}\frac{n^2\pi^2}{n^4*\pi^4-\bar{P_b}*n^2*\pi^2+\bar{K_w}} \tag{22}$$

3. Buckling Analysis of the Modelled Column

In this section of the study, the figures given in Fig. 2. were selected for the sections of the column model to be analyzed. The cross-sectional features may vary according to the analysis.

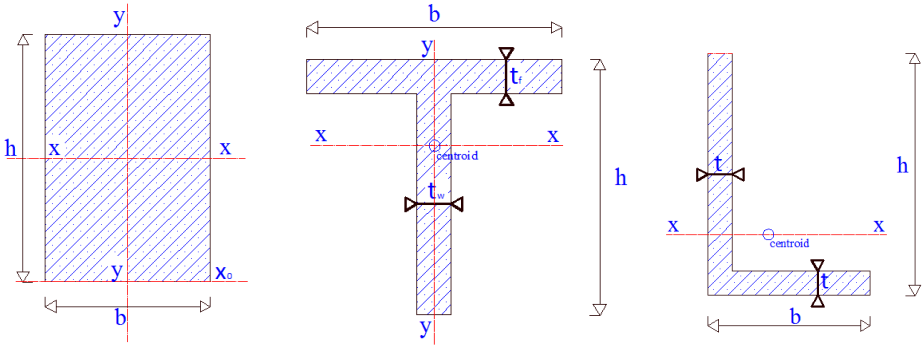

Fig. 2. Rectangular area, Tee section, Angle section, respectively.

The values of the elastic modulus calculated from the stress-strain graph obtained under 28 days pressure loading of each cylinder samples which has dimension of 10x20 cm are shown in Table 1.

Table 1. Elasticity modulus values depending on the type of steel fiber obtained as a result of the experiment.

	C	F30	F35	F50
Elasticity Module (Gpa)	42.56	39.32	36.82	40.97

3.1 The effect of the rotation coefficient on the critical load

The cross-sectional dimensions of the above column are used for the column to be analyzed. In the analysis, the modulus of elasticity was chosen as E=42560 $\frac{N}{mm^2}$ column length L= 3300 mm. 200 terms were used in Stokes' transformations to provide the boundary condition of the

Furier series. The number of terms is valid only for this analysis. The following cross-sectional measurements were used in the analysis: Rectangular area; b=600 mm, h=300 mm; Tee section; t_f=200 mm, t_w=200 mm , h=600 mm, b=600 mm; Angle section b=600 mm, t=200 mm , h=600 mm.

Table 2. Critical load values due to non-rotating spring coefficient (K_w=0.0). (a)

$\overline{\theta_0}=\overline{\theta_L}$	P_{cr} N Rectangular section	P_{cr} N Tee section	P_{cr} N Angle section
0.001	5.20935×10^{7}	1.49206×10^{8}	5.96824×10^{8}
0.01	5.22832×10^{7}	1.49749×10^{8}	5.98998×10^{8}
0.1	5.41618×10^{7}	1.55130×10^{8}	6.20520×10^{8}
0.3	5.82171×10^{7}	1.66745×10^{8}	6.66981×10^{8}
0.5	6.21136×10^{7}	1.77905×10^{8}	7.11622×10^{8}
0.75	6.67711×10^{7}	1.91246×10^{8}	7.64982×10^{8}
1.0	7.12036×10^{7}	2.03941×10^{8}	8.15765×10^{8}
2.0	8.69193×10^{7}	2.48954×10^{8}	9.95816×10^{8}
4.0	1.10729×10^{8}	3.17149×10^{8}	1.26860×10^{9}
10.0	1.49022×10^{8}	4.26828×10^{8}	1.70731×10^{9}
20.0	1.73554×10^{8}	4.97092×10^{8}	1.98837×10^{9}
40.0	1.89774×10^{8}	5.43551×10^{8}	2.17421×10^{9}
80.0	1.99054×10^{8}	5.70130×10^{8}	2.28052×10^{9}
160.0	2.03995×10^{8}	5.84283×10^{8}	2.33713×10^{9}
300.0	2.06370×10^{8}	5.91084×10^{8}	2.36434×10^{9}

Table 3. Critical load values due to non-rotating spring coefficient (K_w=4.9). (b)

$\overline{\theta_0}=\overline{\theta_L}$	P_{cr} N Rectangular section	P_{cr} N Tee section	P_{cr} N Angle section
5	1.22341×10^{8}	3.50410×10^{8}	1.40164×10^{9}
10	1.51423×10^{8}	4.33706×10^{8}	1.73483×10^{9}
15	1.66635×10^{8}	4.77276×10^{8}	1.90911×10^{9}
20	1.75805×10^{8}	5.03540×10^{8}	2.01416×10^{9}
25	1.81888×10^{8}	5.20964×10^{8}	2.08386×10^{9}
30	1.86203×10^{8}	5.33323×10^{8}	2.13329×10^{9}
35	1.89418×10^{8}	5.42529×10^{8}	2.17012×10^{9}
40	1.91902×10^{8}	5.49644×10^{8}	2.19858×10^{9}
45	1.93878×10^{8}	5.55305×10^{8}	2.22122×10^{9}
50	1.95487×10^{8}	5.59913×10^{8}	2.23965×10^{9}
55	1.96822×10^{8}	5.63737×10^{8}	2.25495×10^{9}
60	1.97947×10^{8}	5.66960×10^{8}	2.26784×10^{9}
65	1.98908×10^{8}	5.69713×10^{8}	2.27885×10^{9}
70	1.99739×10^{8}	5.72092×10^{8}	2.28837×10^{9}
75	2.00464×10^{8}	5.74168×10^{8}	2.29667×10^{9}

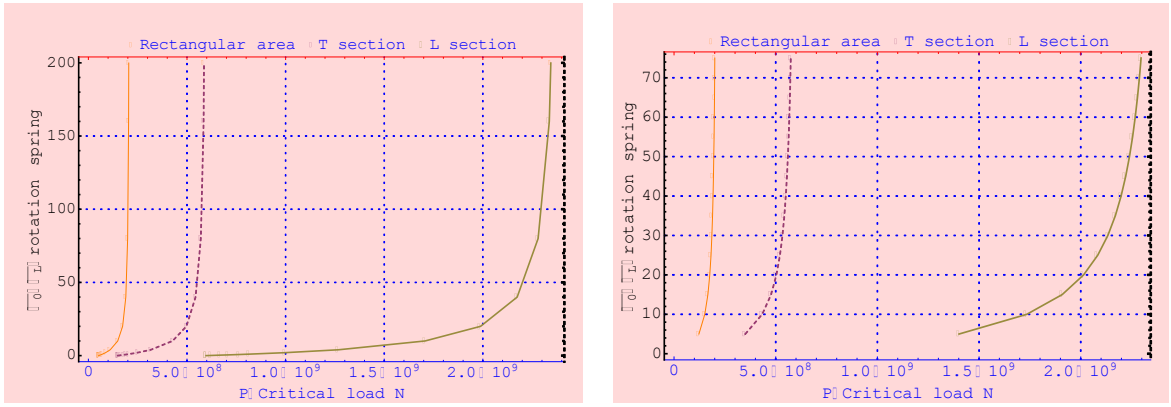

a. b.

Fig. 3. Graph of change in critical load values due to non-rotating spring coefficient.

When graphs and tables are examined, it is seen that the values of the spring ($\overline{\theta_0}$ and $\overline{\theta_L}$) constant which prevent the rotation of the column ends owing to increase the stiffness of the column ends. This increase is a hyperbolically increasing curve from a clamped support to pinned support behavior. Because of the increase in the values taken by the spring constant after a certain point of rigidity, we can call this column clamped-clamped columns. It can be said that the critical load values are examined according to the spring constant that prevents rotation, i.e. according to the boundary condition of the column. As the spring ($\overline{\theta_0}$ and $\overline{\theta_L}$) constant value increased the critical load value increased in the column, likewise as it decreases the critical load decreased. This non-linearly increased critical load reached a maximum critical load point after a certain $\overline{\theta_0}$ and $\overline{\theta_L}$value. At this point, it can be said that both ends of the column are clamped because, as theoretically, the ends are not allowed to rotate.

3.2 Critical load change depending on L/d ratio

For the column model, which is calculated according to the L/d ratio in table 1, the values of A=b.h, inertial radius d=$\sqrt{I/A}$, $\overline{K_L} = 0.0$, b = 600 mm, h = 400 mm were selected for the column model. Modulus of elasticity obtained from the experiment results is E=42560 $\frac{N}{mm^2}$. 150 terms have been used in Stokes transformations to provide the boundary condition of Furier series. The number of terms is valid only for this analysis. The spring constant values ($\overline{\theta_0}$=0.00000001 , $\overline{\theta_L}$=100000000) at the column ends are selected as very high or near zero values for the boundary conditions. Thus, the fixed and clamped support model which is required for the column is obtained.

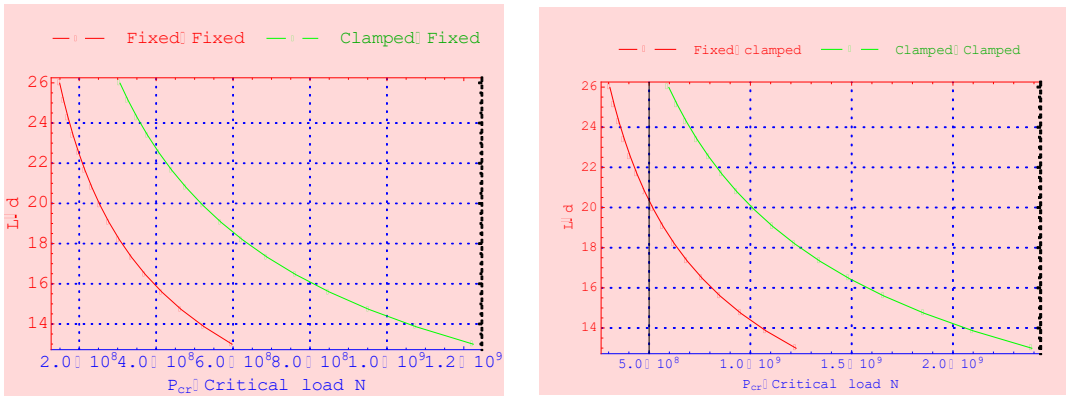

Fig. 4. Critical load graph due to L/d ratio in different boundary conditions.

Table 4. The effect of column thickness on critical load.

L/d	P_{cr} Fixed-Fixed N	P_{cr} Fixed-Clamped N	P_{cr} Clamped-Clamped N
25.9807621	1.49351×10^{8}	3.06361×10^{8}	5.97405×10^{8}
25.1147367	1.59829×10^{8}	3.27853×10^{8}	6.39316×10^{8}
24.2487113	1.71449×10^{8}	3.51690×10^{8}	6.85797×10^{8}
23.3826859	1.84384×10^{8}	3.78223×10^{8}	7.37537×10^{8}
22.5166605	1.98840×10^{8}	4.07877×10^{8}	7.95362×10^{8}
21.6506351	2.15066×10^{8}	4.41159×10^{8}	8.60263×10^{8}
20.7846097	2.33361×10^{8}	4.78689×10^{8}	9.33445×10^{8}
19.9185843	2.54095×10^{8}	5.21219×10^{8}	1.01638×10^{9}
19.0525589	2.77719×10^{8}	5.69679×10^{8}	1.11088×10^{9}
18.1865335	3.04798×10^{8}	6.25226×10^{8}	1.21919×10^{9}
17.3205081	3.36040×10^{8}	6.89312×10^{8}	1.34416×10^{9}
16.4544827	3.72344×10^{8}	7.63780×10^{8}	1.48938×10^{9}
15.5884573	4.14865×10^{8}	8.51002×10^{8}	1.65946×10^{9}
14.7224319	4.65108×10^{8}	9.54064×10^{8}	1.86043×10^{9}
13.8564065	5.25063×10^{8}	1.07705×10^{9}	2.10025×10^{9}
12.9903811	5.97405×10^{8}	1.22544×10^{9}	2.38962×10^{9}

When Table 1 and Fig. 4. are examined, it is seen that increase of L/d ratio causes decrease of critical load value and increase of L/d ratio causes parabolic increase of critical load. ease of critical load value and increase of L/d ratio causes parabolic increase of critical load. The increase in the L/d ratio is result from an increase in column length or a smaller diameter in the cross-sectional area. Increased column diameter or decreased in height reduces the slenderness and therefore it can be said that there will be collapse caused by crushing instead of buckling in the column, because the column will be crushed before reaching the value of excessive critical buckling load. There are limitations in terms of slenderness in the relevant regulations. As can be seen from the limitation of the regulations, with the increase in the column length or the reduction of the column cross-section, the critical load value decreases and this result gives us information about the fact that there is a limit to making high columns with small sections relation with slenderness.

3.3. Critical load change depending on the modulus of elasticity

Table 5 shows the results of the analysis made according to the modulus of elasticity values obtained from the samples in the mixture ratios of different steel fiber previously made for the column model. 3 different cross-sectional types were used in the analysis**.** These sections are from Fig. 2.;

Rectangular : b=900 mm , h=600 mm;
T section : t_f=200 mm , t_w=200 mm, h=600 mm, b=600 mm;
L section (Angle) : b=600 mm , t=200 mm , h=600 mm;
spring coefficients:
$\overline{K_0}$=100000000, $\overline{K_{\mathrm{L}}}$=100000000, $\overline{\theta_0}$=1000000000, $\overline{\theta_{\mathrm{L}}}$=1000000000, $\overline{K_{\mathrm{w}}} = 50.0$

Table 5. Critical load values connected to the E value of different sections with clamped-clamped ends.

I mm^4	E $\frac{N}{mm^2}$	P_{cr} N
1,62x10^{10} (Rectangular)	42560	1.53916×10^9
	40970	1.42202×10^9
	39320	1.33163×10^9
	36820	1.48167×10^9
3.86667×10^9 (T section)	42560	3.67456×10^8
	40970	3.39485×10^8
	39320	3.17901×10^8
	36820	3.53730×10^8
1.54667×10^{10} (L section)	42560	1.46951×10^9
	40970	1.35767×10^9
	39320	1.27137×10^9
	36820	1.41462×10^9

spring coefficients:

$\overline{K_0}$=100000000, $\overline{K_L}$=100000000, $\overline{\theta_0}$=1000000000, $\overline{\theta_L}$1000000000, $\overline{K_w} = 0.0$;

Table 6. Critical load values connected to the E value of different sections with pinned-pinned ends.

I mm^4	E $\frac{N}{mm^2}$	P_{cr} N
1,62x10^{10} (Rectangular)	42560	2.74811×10^9
	40970	2.64545×10^9
	39320	2.53891×10^9
	36820	2.37748×10^9
3.86667×10^9 (T section)	42560	6.55928×10^8
	40970	6.31424×10^8
	39320	6.05994×10^8
	36820	5.67464×10^8
1.54667×10^{10} (L section)	42560	2.62371×10^9
	40970	2.52569×10^9
	39320	2.42398×10^9
	36820	2.26986×10^9

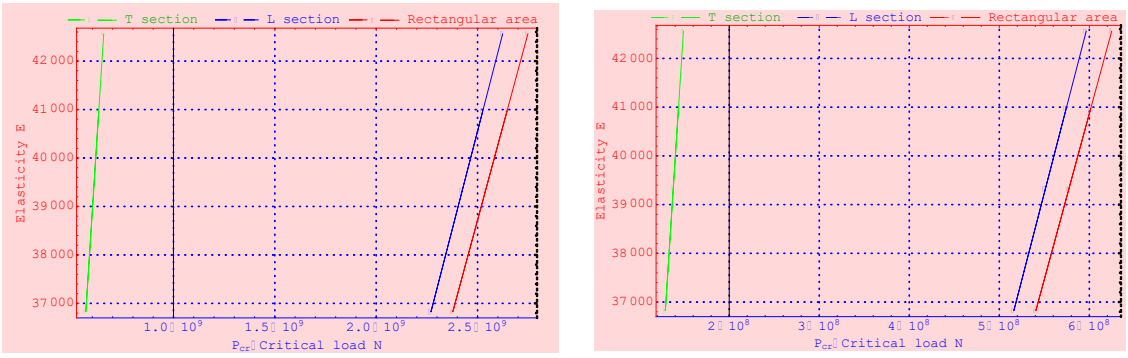

Clamped-clamped ends (K_w = 50). Pinned-pinned ends (K_w = 0).

Fig. 5. Critical load graphs connected to the Elasticity module in different section types of columns.

When Fig. 5. Table 5. and Table 6. are examined, it is seen that the increase of the modulus of elasticity increases the critical load value linearly.

3.4. Critical load value depending on the column length

Table 5 shows the critical load values of 3 different section types in column-length analysis. Spring coefficients for the column model**:**

$\overline{\theta_0}$=0.000000001, $\overline{\theta_L}$=0.0000000001, $\overline{K_0}$=10000000, $\overline{K_L}$= 10000000 $\overline{K_w} = 50.0$.

Modulus of elasticity obtained from the experiment results is E=42000 $\frac{N}{mm^2}$. 150 terms were used in the analysis.
Measurements of the sections to be used in the analysis:
Rectangular : b=600 mm , h=400 mm;
Tee section : t_f=200 mm , t_w=200 mm, h=600 mm, b=600 mm;
L section (Angle) : b=400 mm , t=200 mm , h=400 mm

Table 7. Table of critical load change due to column length of different sections with clamped-clamped ends.

Column Length mm	P_{cr} N Rectangular Area	P_{cr} N T section	P_{cr} N Angle section
3000	6.56833×10^8	7.93673×10^8	9.85249×10^8
3300	5.42837×10^8	6.55928×10^8	8.14256×10^8
3600	4.56134×10^8	5.51162×10^8	6.84201×10^8
3900	3.88659×10^8	4.69629×10^8	5.82988×10^8
4200	3.35119×10^8	4.04935×10^8	5.02678×10^8
4500	2.91926×10^8	3.52744×10^8	4.37889×10^8
4800	2.56575×10^8	3.10029×10^8	3.84863×10^8
5100	2.27278×10^8	2.74627×10^8	3.40917×10^8
5400	2.02726×10^8	2.44961×10^8	3.04089×10^8
5700	1.81948×10^8	2.19854×10^8	2.72922×10^8
6000	1.64208×10^8	1.98418×10^8	2.46312×10^8

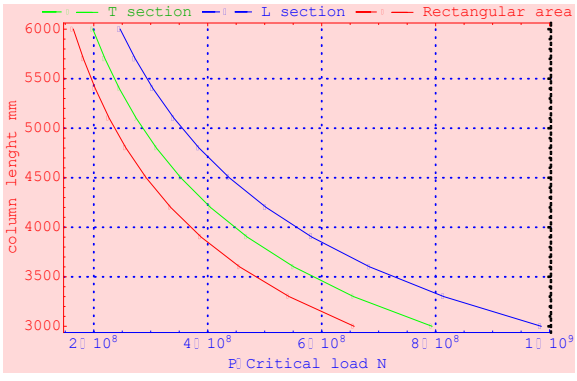

Fig. 6. Critical load variation due to column length of different sections with clamped-clamped ends.

Table 7. and Fig 6. shows that the effect of column length on critical load is not linear. Increasing the column length causes a hyperbolic reduction of the load capacity as it makes the column delicate.

3.5. Critical load disribution due to modulus of elasticity

Three different cross-sectional types were used in the analyzes. $\bar{K_w} = 0.0$ is selected spring coefficient for elastic restrained and $L = 3300$ is selected for column length. Table 8 shows critical buckling values depending on the values given. Similarly, Table 9. shows the results of the critical buckling load to be obtained when the L=3300, $\overline{K_w}$=50.0, $\overline{P_b}$=(P_{cr} L^2)/(E I), $\overline{K_0}$=10000000, $\overline{K_L}$=10000000, $\overline{\theta_0}$=10000000, $\overline{\theta_L}$=100000000 values are used for the column model to be analyzed. In the same way, table 8. shows the moment of inertia that is based on section dimensions, elasticity modules and section dimensions. The graph of the critical buckling values found in figure 7 is shown.

Table 8. Critical load distribution table of the different sections connected to the modulus of elasticity with fixed-fixed ends.

I mm^4	sectional dimensions (bxh) mm	P_{cr} N (E = 36820 N/mm^2)	P_{cr} N (E = 39320 N/mm^2)	P_{cr} N (E = 40970 N/mm^2)	P_{cr} N (E = 42560 N/mm^2)
1,350x10^9	**(600*300)**	4.50494×10^7	4.81082×10^7	5.0127×10^7	5.20724×10^7
3,200x10^9	**(600*400)**	1.06784×10^8	1.14034×10^8	1.1882×10^8	1.23431×10^8
6,250x10^9	**(600*500)**	2.08562×10^8	2.22723×10^8	2.32069×10^8	2.41076×10^8
1,080x10^{10}	**(600*600)**	3.60396×10^8	3.84866×10^8	4.01016×10^8	4.16579×10^8
1,715x10^{10}	**(600*700)**	5.72295×10^8	6.11152×10^8	6.36798×10^8	6.61512×10^8
2,560x10^{10}	**(600*800)**	8.54271×10^8	9.12274×10^8	9.50556×10^8	9.87446×10^8

Table 9. Critical load distribution table of the different sections connected to the modulus of elasticity with clamped-clamped ends.

I mm^4	sectional dimensions (bxh) mm	P_{cr} N (E = 36820 N/mm^2)	P_{cr} N (E = 39320 N/mm^2)	P_{cr} N (E = 40970 N/mm^2)	P_{cr} N (E = 42560 N/mm^2)
1,350x10^9	**(600*300)**	1.98116×10^8	2.11568×10^8	2.20446×10^8	2.29001×10^8
3,200x10^9	**(600*400)**	4.69609×10^8	5.01495×10^8	5.22539×10^8	5.42818×10^8
6,250x10^9	**(600*500)**	9.17206×10^8	9.79482×10^8	1.02058×10^9	1.06019×10^9
1,080x10^{10}	**(600*600)**	1.58493×10^9	1.69254×10^9	1.76357×10^9	1.83201×10^9
1,715x10^{10}	**(600*700)**	2.51681×10^9	2.68770×10^9	2.80048×10^9	2.90917×10^9
2,560x10^{10}	**(600*800)**	3.75687×10^9	4.01196×10^9	4.18031×10^9	4.34255×10^9

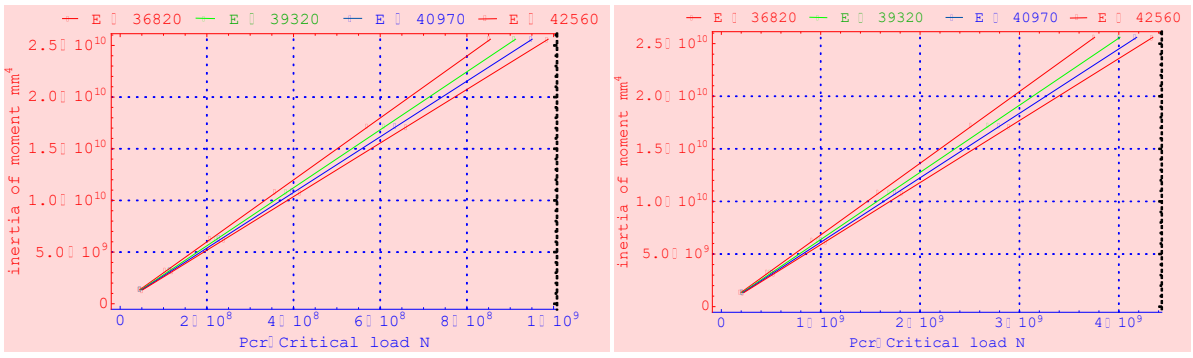

(a) Fixed-fixed (b) Clamped-clamped

Fig. 7. Critical load distribution table of the different sections connected to the modulus of elasticity.

Table 9. and Fig 7. shows that the increase in the section width leads to an increase in the critical load value. Similarly, the increase in the modulus of elasticity of the material also increased the value of the critical load.

4. Conclusion

In the study, the buckling analysis of the Euler column model with different boundary conditions, which was elastically limited a column model, with the help of Stokes' transformations and Fourier sine series which had been previously proposed by the researchers, was done. In the analysis, elasticity modulus values of the steel fiber reinforced and non-fibrous concrete specimens with different mixing ratios obtained from the experimental results were used. The status of three different sections was examined. The result show that:

- Because of increased column diameter or decrease in the length of the column, the critical buckling load values in the column increased hyperbolically. For this reason, very large critical buckling load values are obtained. This indicates that the crush will occur due to pressure load before a buckling occurs after a certain critical load value in the column. Regarding this, restrictions have been made in terms of delicacy in the regulations. In other words, with the increase in column length or narrowing of the diameter, the critical load value decreases and this result gives us information about the fact that there is a limit to making high columns with small sections.

- Since the value of the modulus of elasticity obtained from the non-fibrous concrete (C) mixture is the highest value, the highest value of the critical load is seen in this sample. Then the greatest critical load values were seen in F50, F30, and F35, respectively.

Acknowledgment

The authors gratefully acknowledge support provided by Bursa Uludag University Scientific Research Projects Centre (BAP) under grant numbers KUAP(MH)-2017/11.
The authors would like to thank Bursa-Beton Ready Mixed Concrete Plant and Polisan Construction Chemicals Company authorities for their kind assistance in providing the cement, superplasticizer admixture and fiber as well as determining the chemical composition of these products.

References

[1] Euler, L., De curvis elasticis. In Methodus inveniendi leneas curva maximi minimive proprietate gaudentes, sive solutio problematis isoperimetrici lattisimo sensu accepti, Lausannae, E65A. O. O. Ser.I., 24, 231-297, 1744.

[2] Brush, D. O., Almroth, B. O., Buckling of Bars, Plates and Shells, McGraw-Hill Comp., 1975.

[3] Dinnik, A. N., Design of columns of varying cross section. Trans ASME, 51(1), 105-14, 1929.

[4] Keller, J. B., The shape of the strongest column. Archive for Rational Mechanics and Analysis, 5(1), 275-285, 1960.

[5] Tadjbakhsh, I., & Keller, J. B. Strongest columns and isoperimetric inequalities for eigenvalues. Journal of Applied Mechanics, 29(1), 159-164, 1962.

[6] Taylor, J. E., The strongest column: an energy approach. Journal of Applied Mechanics, 34(2), 486-487, 1967.

[7] Timoshenko, S., Theory of elastic stability 2e. Tata McGraw-Hill Education, 1970.

[8] Lee, G.C., Morrell, M.L. and Ketter, R.L., "Design of Tapered Members" Welding Research Council, Bulletin #173, June 1972.

[9] Lee, G.C., Chen, Y.C. and Hsu, T.L., "Allowable Axial Stress of Restrained Multi-Segment, Tapered Roof Girders." Welding Research Council, Bulletin #248, May 1979.

[10] Lee, G.C. and Hsu, T.L., "Tapered Columns with Unequal Flanges." Welding Research Council, Bulletin #272, November 1981.

[11] Lee, G.C., Ketter, R.L. and Hsu, T.L., "Design of Single Story Rigid Frames", Metal Building Manufacturer's Association, Cleveland, Ohio, 1981.

[12] Li, Q., Cao, H., & Li, G., Stability analysis of a bar with multi-segments of varying cross-section. Computers & structures, 53(5), 1085-1089, 1994.

[13] Qiusheng, L., Hong, C., & Guiqing, L., Stability analysis of bars with varying cross-section. International Journal of Solids and Structures, 32(21), 3217-3228, 1995.

[14] Li, Q., Cao, H., & Li, G., Static and dynamic analysis of straight bars with variable cross-section. Computers & structures, 59(6), 1185-1191, 1996.

[15] Kim, H. K., Kim, M. S., Vibration of beams with generally restrained boundary conditions using Fourier series. Journal of Sound Vibration 245(5):771–784. doi: 10.1006/jsvi.2001.3615, 2001.

[16] Atay, M. T., & Coşkun, S., Elastic stability of Euler columns with a continuous elastic restraint using variational iteration method. Computers & Mathematics with Applications, 58(11-12), 2528-2534, 2009.

[17] Coşkun, S. B., & Atay, M. T., Determination of critical buckling load for elastic columns of constant and variable cross-sections using variational iteration method. Computers & Mathematics with Applications, 58(11-12), 2260-2266, 2009.

[18] Singh, K. V., & Li, G., Buckling of functionally graded and elastically restrained non-uniform columns. Composites Part B: Engineering, 40(5), 393-403, 2009.

[19] Yao, F., Meng, W., Zhao, J., She, Z., & Shi, G., Analytical method comparison on critical force of the stepped column model of telescopic crane. Advances in Mechanical Engineering, 10(10), 1687814018808697, 2018.

[20] Atay, M. T. Determination of buckling loads of tilted buckled column with varying flexural rigidity using variational iteration method. International Journal of Nonlinear Sciences and Numerical Simulation, 11(2), 97-104, 2010.

[21] Okay, F., Atay, M. T., & Coşkun, S. B. Determination of buckling loads and mode shapes of a heavy vertical column under its own weight using the variational iteration method. International Journal of Nonlinear Sciences and Numerical Simulation, 11(10), 851-858, 2010.

[22] Al-Kamal, M. K., Estimating Elastic Buckling Load for an Axially Loaded Column Bolted to a Simply Supported Plate using Energy Method. Alnahrain journal for engineering sciences, 20(5), 1154-1159, 2017.

[23] Yilmaz, Y., Girgin, Z., & Evran, S., Buckling analyses of axially functionally graded nonuniform columns with elastic restraint using a localized differential quadrature method. Mathematical Problems in Engineering, 2013.

[24] Ofondu, I. O., Ikwueze, E. U., & Ike, C. C., Determination of the critical buckling loads of euler columns using stodola-vianello iteration method. Malaysian Journal of Civil Engineering, 30(3), 2018.

[25] Coşkun, S. B., Determination of critical buckling loads for euler columns of variable flexural stiffness with a continuous elastic restraint using homotopy perturbation method. International Journal of Nonlinear Sciences and Numerical Simulation, 10(2), 191-198, 2009.

[26] Başbük, M., Eryılmaz, A., & Atay, M. T., On Critical Buckling Loads of Columns under End Load Dependent on Direction. International scholarly research notices, 2014.

[27] Basbuk, M., Eryilmaz, A., Coskun, S. B., & Atay, M. T., On Critical Buckling Loads of Euler Columns With Elastic End Restraints. Hittite Journal of Science & Engineering, 3(1), 2016.

[28] Pinarbasi, S., Stability analysis of nonuniform rectangular beams using homotopy perturbation method. Mathematical Problems in Engineering, 2012, 2012.

[29] Mercan, K., & Civalek, Ö., Buckling analysis of Silicon carbide nanotubes (SiCNTs) with surface effect and nonlocal elasticity using the method of HDQ. Composites Part B: Engineering, 114, 34-45, 2017.

[30] Civalek, Ö., & Demir, C., Buckling and bending analyses of cantilever carbon nanotubes using the euler-bernoulli beam theory based on non-local continuum model. Asian Journal of Civil Engineering, 12(5), 651-661, 2011.

[31] Akgöz, B., & Civalek, Ö., Buckling analysis of functionally graded microbeams based on the strain gradient theory. Acta Mechanica, 224(9), 2185-2201, 2013.

[32] Yayli, M. Ö., Buckling analysis of a microbeam embedded in an elastic medium with deformable boundary conditions. Micro & Nano Letters, 11(11), 741-745, 2016.

[33] Yayli, M. Ö., Buckling analysis of a cantilever single-walled carbon nanotube embedded in an elastic medium with an attached spring. Micro & Nano Letters, 12(4), 255-259, 2017.

[34] Yaylı, M. Ö., Stability analysis of gradient elastic microbeams with arbitrary boundary conditions. Journal of Mechanical Science and Technology, 29(8), 3373-3380, 2015.

[25] Robinson, M. T. A., & Adali, S., Buckling of nonuniform and axially functionally graded nonlocal Timoshenko nanobeams on Winkler-Pasternak foundation. Composite Structures, 206, 95-103, 2018.

[36] Akgöz, B., & Civalek, Ö., Strain gradient elasticity and modified couple stress models for buckling analysis of axially loaded micro-scaled beams. International Journal of Engineering Science, 49(11), 1268-1280, 2011.

[37] Huang, Y., Yang, L. E., & Luo, Q. Z., Free vibration of axially functionally graded Timoshenko beams with non-uniform cross-section. Composites Part B: Engineering, 45(1), 1493-1498, 2013.

[38] Huang, Y., & Luo, Q. Z., A simple method to determine the critical buckling loads for axially inhomogeneous beams with elastic restraint. Computers & Mathematics with Applications, 61(9), 2510-2517, 2011.

[39] Nejad, M. Z., Hadi, A., & Rastgoo, A., Buckling analysis of arbitrary two-directional functionally graded Euler–Bernoulli nano-beams based on nonlocal elasticity theory. International Journal of Engineering Science, 103, 1-10, 2016.

[40] Pinarbasi, S., Buckling analysis of nonuniform columns with elastic end restraints. Journal of Mechanics of Materials and Structures, 7(5), 485-507, 2012.

[41] Şimşek, M., Buckling of Timoshenko beams composed of two-dimensional functionally graded material (2D-FGM) having different boundary conditions. Composite Structures, 149, 304-314, 2016.

[42] Gül, U., Aydoğdu, M., & Edirme, E., Elastik Zemin Üzerinde Oturan Timoshenko Kirişlerinde Dalga Yayınımı, 2015.

[43] Zhang, Y., Zhang, L. W., Liew, K. M., & Yu, J. L., Buckling analysis of graphene sheets embedded in an elastic medium based on the kp-Ritz method and non-local elasticity theory. Engineering Analysis with Boundary Elements, 70, 31-39, 2016.

[44] Yayli, M. Ö., Buckling analysis of Euler columns embedded in an elastic medium with general elastic boundary conditions. Mechanics *Based Design of Structures and Machines*, *46*(1), 110-122, 2018.

[45] Timoshenko, S. P., & Gere, J. M., Theory of elastic stability, 1961.

[46] Wang, C. M., & Wang, C. Y., Exact solutions for buckling of structural members (Vol. 6). CRC press, 2004.

International Journal of Engineering & Applied Sciences (IJEAS)
Vol.11, Issue 1 (2019) 345-368
http://dx.doi.org/10.24107/ijeas.555719
Int J Eng Appl Sci 11(1) (2019) 345-368

A Review on Buckling Analysis of Functionally Graded Plates Under Thermo-Mechanical Loads

Ahmed Hassan Ahmed Hassan [a*], *Naci Kurgan* [b]

[a,b] *Ondokuz Mayis University, Faculty of Engineering, Department of Mechanical Engineering, Samsun, Turkey.*
E-mail address: 15210457@stu.omu.edu.tr [a*], naci.kurgan@omu.edu.tr [b]

ORCİD numbers of authors
0000-0002-4880-0184 [a], 0000-0001-7297-7249 [b]

Received date: 18.04.2019
Accepted date: 21.05.2019

Abstract

Functionally graded materials (FGM) are increasingly used in the engineering field. In many applications, FGMs are modelled as plates. Plates made of functionally graded materials (FGPs) are mostly designed to perform under elevated temperatures. In those circumstances, they are often under the combined effect of thermal and mechanical loads. There have been many studies on buckling analysis of FGP under either mechanical or thermal loads; however, only a few studies have addressed the combined effect of both loads acting together. This article focuses on the review of research on buckling analysis of FGP under the combined thermal and mechanical loads.

Keywords: Functionally graded material; plate; FGP models; thermo-mechanical buckling; solution methods.

1. Introduction

Functionally graded materials (FGMs) are advanced inhomogeneous composite materials in which graded interlayer separates different materials of the composite structure. FGM's concept is to replace the sudden change in composition that occurs at the interface between different materials, with a compositionally graded phase, aiming at reducing stress concentrations through the structure. This microstructure variation in FGM occurs with a specific function through one or more dimensions of the volume. The concept of gradual variation in material is found in nature. Many organic structures have gradual variation through one or more dimensions. For example, human bones and bamboo trees. More examples are available in [1]. FGM's concept was first explored theoretically early in the seventies of the previous century by Shen and Bever [2, 3]. More than ten years later, in Japan, 1984, FGM concept was first implemented in engineering application. That first implementation was in design of thermal-resistant structure. Since then there have been intensive research and various implementations of FGM concept in various engineering applications. Recently, FGM has been introduced to gear structures [4, 5], turning tools [6], drilling wicks [7] and many other applications including tubes, rotating disks and sport instruments [8]. In addition, FGMs have found applications as

electrical field grading insulators [9]. Other important applications of FGMs are in the medical field. FGMs have been intensively investigated as biomaterials [10, 11], especially in dentistry as dental implants and crowns [12, 13], bone plates [14], bone implants [15] and knee joints [16].

In literature, there are various methods of modeling, analysis, fabrication and characterizing of FGM parts available. Relatively thin structures with a wide flat planar surface are normally called plates. When the concept of FGM is implemented to a plate then it is called functionally graded plate (FGP). FGPs are generally designed to withstand high thermal loads and it often experiences some additional mechanical loads. Therefore, FGPs often have to be designed to withstand the combined effect of the thermal and mechanical loads. FGPs provide designers with the ability to tailor material response so desired performance can be achieved. FGPs found wide range of applications especially space vehicles where it was first implemented [1]. Other fields also have started to adopt and benefit from this relatively new concept. As an example, Cooley [17] designed an exhaust wash structure as FGP to be used in aircrafts those have internally exhausted engines. There have been many studies on analysis of FGP under either mechanical or thermal loads; however, only a few studies have addressed the combined effect of both loads acting together. One main analysis usually conducted in plate design is buckling analysis. When a flat plate experiences compressive in-plane loads, resulting from compression loads at its edges or thermal loads with constrained edges, buckling and post-buckling analysis have to be conducted to ensure correct prediction of the plate's behavior. Review articles those cover FGP buckling under combined thermal and mechanical loads are rare. Swaminathan [18] reviewed thermo-mechanical buckling analysis of FGPs briefly in a subsection of a wide review that also contains stress and vibration analysis. Later on, same author, Swaminathan [19] reviewed modeling and solution methods used in thermal buckling of FGPs, but did not separate buckling under combined thermal and mechanical loads from thermal buckling studies. It is obvious that the combined loading is the general case. Therefore, focusing on it and showing which FGPs' models, shapes, configurations and solution methods are used is a step towards filling gaps in this study field.

In this review article, FGP buckling under combined thermal and mechanical loads studies are reviewed aiming at providing a closer look at this specific analysis and pointing at existing gaps in its literature. This review starts with brief on FGP definition as a plate and as functionally graded material and about their geometries and configurations, those appear in literature. Then, in the third section, the implemented models are listed with brief description. Followed by the fourth section briefing methods to characterize FGP properties. In the fifth section, buckling, thermal buckling and thermo-mechanical buckling are briefly discussed. Solution methods are reviewed in the sixth section. Suggestions and comments are included in the last section.

2. FGP definition, shapes and configuration

FGP is a plate that has the concept of FGM implemented to its composition. Reddy [20] defined plate as: "A plate is a structural element with planform dimensions that are large compared to its thickness and is subjected to loads that cause bending deformation in addition to stretching". A rectangular plate is shown in Fig. 1 with typical coordinate system and names of characteristic dimensions. Normally, the length of the longer inplane edge of the plate is referred to as (a), where the shorter is referred to as (b), while the out-of-plane depth, a.k.a. thickness, is referred to as (h).

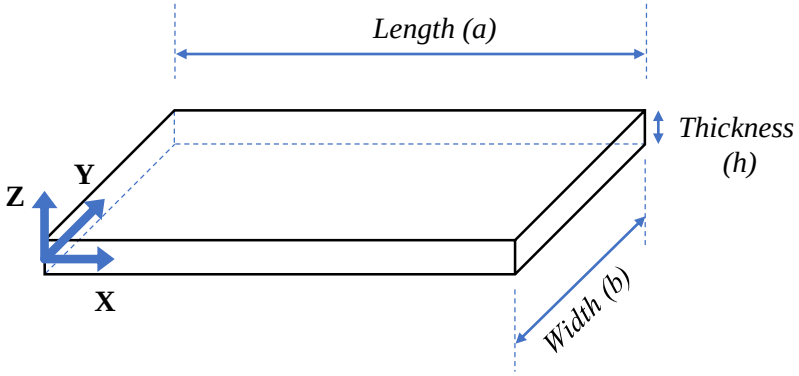

Fig. 1. Rectangular plate structure

In literature, various shapes and configurations are considered in thermo-mechanical buckling analysis of FGPs. Different shapes and configurations come from the many aspects those define a FGP as a plate and those define FGP as FGM.

2.1. FGP's plate characteristics

The first aspect that defines FGP as a plate is its thickness to side ratio. Plates may be classified according to the ratio of a its typical inplane dimension to its thickness [21] into thick, moderately thick and thin plates. All the three classes have been found in literature of thermo-mechanical buckling analysis of FGPs. Few examples for studies that considered thin plates are [22] and [23]; moderately thick plates [24] and [25]; and thick plates [26] and [27]. Another aspect is the thickness variation; in the literature under focus, only FGPs with constant thickness were found. Next aspect for defining a plate is the scale of its dimensions. According to this aspect, FGP can be classified into nano-plates, micro- plates and "normal" plates. Nano-FGP and micro-FGPs have been studied for thermo-mechanical buckling by many researchers, for example [28]. Nano-FGP and micro-FGP are out of the scope of this review article.

Next aspect is the shape of the FGP. The rectangular is the most studied shape of FGP for the thermo-mechanical buckling analysis. However, other FGP shapes have been also studied. Other considered shapes are the annular FGP analyzed numerically by Shariyat [29], skew FGP analyzed numerically by Taj [30] and Yu [31], square FGP analyzed by Kowal-Michalska [22] using approximate analytical method, and circular FGP studied by Kiani [32], Fallah [33] and Li [34]. Various special configurations have been considered in literature. Stiffened FGPs have been studied by Cong [25], Van [35] and Duc [27]. FGP with holes and perforated FGP have been considered by Lal [36] and Shariyat [29], respectively. Porous FGP have been analyzed by Cong [37] using approximate analytical methods. Cracked FGP have been analyzed by Fan [38] using approximate analytical methods.

2.2. FGP resting on elastic foundation

An important configuration is FGP resting on elastic foundation. The simplest model for the elastic foundation is the Winkler model, which regards the foundation as a series of separated springs without coupling effects between each other. Pasternak model adds a shear layer to the Winkler model as a parameter. Pasternak model is widely used to describe the mechanical behavior of structure–foundation interactions [39]. More complicated foundation model is Kerr's model, which adds a third parameter as an additional shear layer [40].

In the literature of thermo-mechanical buckling analysis of FGP, the only used foundation model is the Pasternak model. FGP on Pasternak foundation has been analyzed using approximate analytical methods by Cong [25, 37], Bakora [26], Duc [27, 41], Bateni [42], Chikh [43], Yu [44], Fan [38] and Shen [45, 46]. Whereas Mansouri [47] and Shams [48] used numerical methods. It is worth mentioning that in all these studies only the rectangular plate was considered.

2.3. Sandwich FGP

Lastly, we have sandwich FGP configuration. FGP may be included in sandwich structure as core material or as face sheet material as shown in Fig. 2. In literature of thermo-mechanical buckling analysis, both structures have been considered and studied. Tung [24], Yu [44], Shen [45, 46, 49] and Yaghoobi [50] studied various FGP sandwich configurations. It is noticed that all these studies implemented approximate analytical methods. In addition, all of these studies considered only the rectangular FGP.

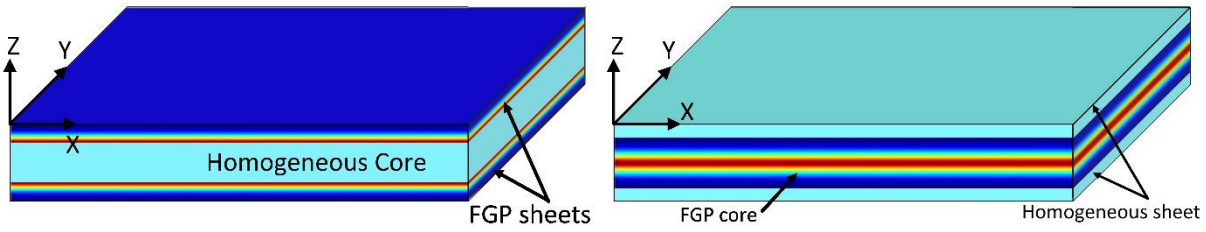

a) FGM sheets on homogenous core b) Homogenous sheets on FGM core

Fig. 2. Sandwich FGP structures

2.4. FGP's FGM characteristics

The second part of aspects define FGP as FGM. The first aspect in this part is the dimensionality of FGP, which refers to the number of dimensions through which properties variation occurs. Composition variation happens through the thickness, or the in-plane two dimensions [51, 52] as shown in Fig. 3. In literature of thermo-mechanical buckling analysis of FGP, the only studied FGP is the 1-D that has its variation through the thickness.

The Next aspect is the symmetry of variation of FGP. Generally, in thermal buckling analysis, the plate symmetry is important in determining if there will be a bifurcation point or not. Fig. 4 shows a symmetric and non-symmetric rectangular FGPs. Lack of symmetry is considered as serious initial imperfection in the plate, that prevent reaching a bifurcation point except for specific loading configurations and boundary conditions. Examples for studies considered symmetric FGP: [24, 43, 49, 50, 53, 54]; and for non-symmetric FGPs: [22, 38, 42, 44].

Another important aspect is the continuity of the variation in FGP. FGP may be studied as single layer with continuous variation with a function determines its properties at every point of the plate, or as laminated homogenous layers with specific thickness of each, as shown in Fig. 5. Usage of one of these models depends on the solution methods.

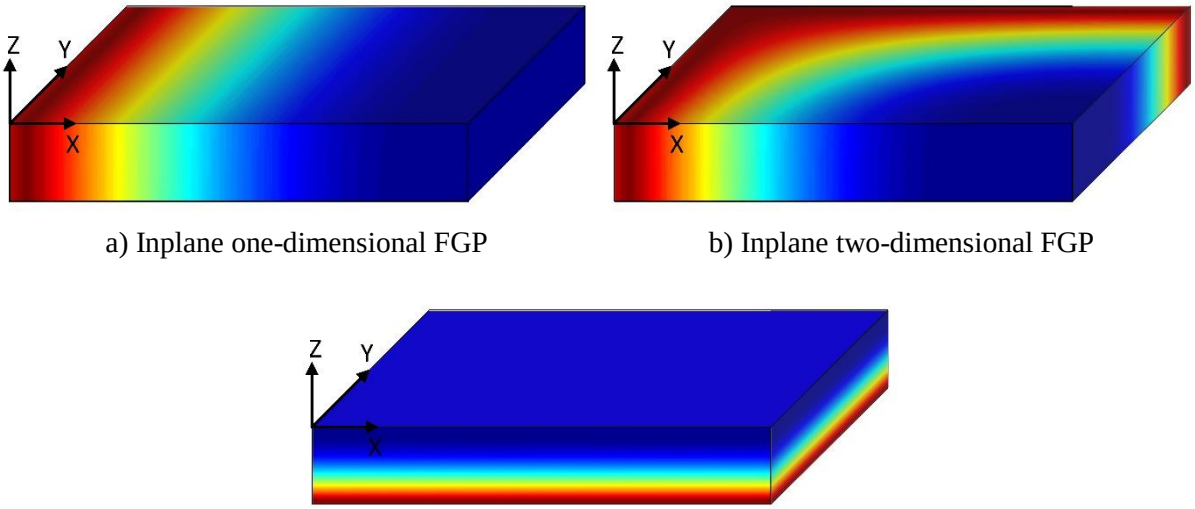

a) Inplane one-dimensional FGP

b) Inplane two-dimensional FGP

c) Out-of-plane one-dimensional FGP

Fig. 3. FGP's property/composition variation dimensionality

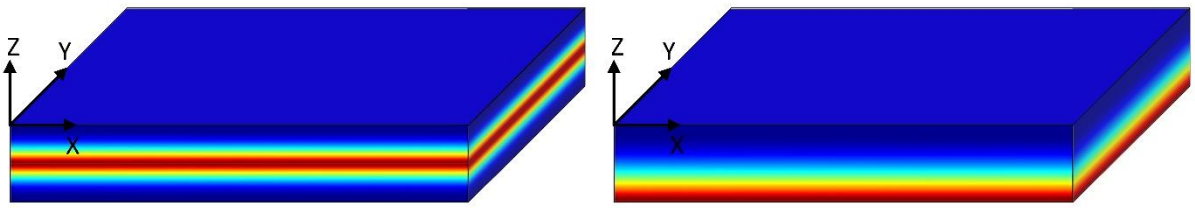

a) Symmetric FGP

b) Non-symmetric FGP

Fig. 4. Symmetry of FGP

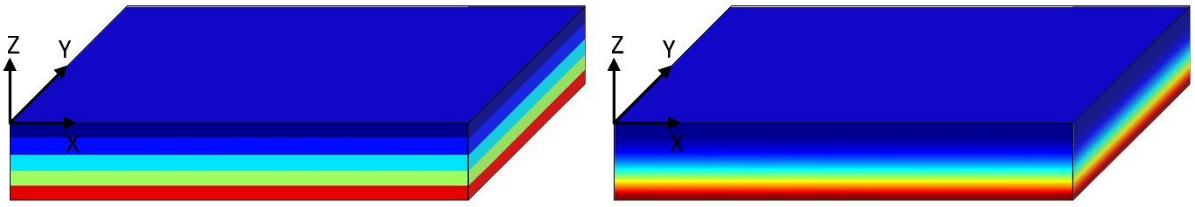

a) Stepped (laminated) FGP

b) Continuous FGP

Fig. 5. Variation continuity of FGP

3. FGP models

Modelling and Analysis of FGPs' behavior are discussed in many books of plate mechanics, e.g. [20, 21, 55-62]. Thermo-mechanical buckling of FGPs has been studied mostly using various models based on plate theories. However, other models based on theory of elasticity are rarely used for this analysis. Following is a brief on the models used in thermo-mechanical buckling of FGPs.

3.1. Models based on elasticity theory

Theory of elasticity is based on the concepts of equilibrium, continuum and a material constitutive relationship to analyze any structure [58]. While FGPs can be analyzed using elasticity theory providing high accuracy solutions, it requires more solving effort in both analytical and numerical solution methods. Using elasticity theory to analyze plates provide benchmark to assess accuracy and validity of other simplified methods [63]. In literature of thermo-mechanical buckling analysis of FGP, an elasticity theory-based model has been used just once in the recent study of Shariyat [29].

3.2.Models based on plate theories

Plate theories are based on mechanics-of-material approach. Mechanics-of-material approach is based on assuming suitable hypothesis regarding the geometry of deformation, which simplify the problem resulting in simpler models [20]. Models based on plate theories contain equivalent single layer (ESL) models and laminated layer models. In literature of FGP thermo-mechanical buckling, laminated layer model has been used just once by Kowal-Michalska [22]. Equivalent Single Layer theories (ESL) are based on the assumption that properties, and hence displacement, through the thickness of the plate can be expressed by a function. This function may be polynomial or non-polynomial. Because of the smallness of the plate thickness, it is suitable to analysis the plate as two-dimensional structure with assumed relations describe variation of deformation and stresses through the thickness. comprehensive view of ESL is presented at [64]. ESL-based models those used in thermo-mechanical buckling analysis of FGPs are briefly described as follows.

3.2.1. Classical plate theory (CPT)

This theory was developed in 1888 by Love using assumptions proposed by Kirchhoff. It is also called "Kirchhoff plate theory", "Kirchhoff-Love plate theory" or "Thin plate theory". It is an extension of "Euler–Bernoulli beam theory". CPT ignores both shear and normal deformation effects. Assumptions of this theory are expressed as restrictions of transverse normals, i.e. straight lines normal to the mid-surface before deformation. CPT assumes that transverse normals remain straight, normal to the neutral plane and at the same length after deformation [20]. Displacement field of the CPT can be written as shown in Eq. (1), in which (u, v, w) are the displacements of any point (x, y, z) of the plate in X, Y and Z-directions respectively; (u_0, v_0, w_0) are the displacements of point (x, y) at the neutral plane in X, Y and Z-directions respectively. CPT models are implemented in FGP thermo-mechanical buckling analysis by Amoushahi [65] for rectangular FGP. In addition to buckling, post-buckling has been studied using CPT model by Tung [66] for rectangular FGP and Li [34] for circular FGP.

$$u(x,y,z) = u_0(x,y) - z\frac{\partial w_0}{\partial x}$$
$$v(x,y,z) = v_0(x,y) - z\frac{\partial w_0}{\partial y} \quad (1)$$
$$w(x,y,z) = w_0(x,y)$$

3.2.2. First order shear deformation theory (FSDT)

Also called "Reissner-Hencky-Bollé-Mindlin plate Theory", "Reissner-Mindlin plate Theory", "Mindlin plate Theory", "first-order theory" or "Moderately thick plate theory" [58]. It forms an extended version of "Timoshenko beam theory". FSDT extends the CPT by relaxing the normality restriction of the transverse normals to the neutral plane. FSDT assumes that transverse normals remain straight and at the same length after deformation. FSDT yields a constant value of transverse shear strain through the thickness of the plate, and thus requires shear correction factors to account for the parabolic distribution of shear strain [20]. Displacement field of the FSDT can be written as shown in Eq. (2).

$$u(x,y,z) = u_0(x,y) + z\,\phi_x(x,y)$$
$$v(x,y,z) = v_0(x,y) + z\,\phi_y(x,y) \quad (2)$$
$$w(x,y,z) = w_0(x,y)$$

(u,v,w) are the displacements of any point (x,y,z) of the plate in X, Y and Z-directions respectively; (u_0,v_0,w_0) are the displacements of point (x,y) at the neutral plane in X, Y and Z-directions respectively; (ϕ_x,ϕ_y) are the rotations of a transverse normal about the Y- and X-axes, respectively. FSDT models are implemented in FGP thermo-mechanical buckling analysis in [23-25, 31, 33, 48, 50, 53, 67-72] for rectangular FGPs and in [73] for circular FGP.

3.2.3. Higher order shear deformation theory (HSDT)

Also called refined nonlinear theory of plates. In order to eliminate the need for shear correction factor needed for FSDT, higher shear deformation theories were proposed. In addition, HSDT yields more accurate results than FSDT along with more computational efforts. Theoretically, shear deformation order may reach any order to achieve desired degree of accuracy; but in practice, the third order shear deformation is quite enough giving satisfying results with affordable computational effort. There are many third-order shear deformation theories (TSDT), but the most widely used is Reddy's TSDT, proposed by Reddy [74]. Third order shear deformation theories are reviewed in [75]. Displacement field of the TSDT can be written as shown in Eq. (3).

$$u(x,y,z) = u_0(x,y) + z\,\psi_x(x,y) + z^2\xi_x(x,y) + z^3\,\zeta_x(x,y)$$
$$v(x,y,z) = v_0(x,y) + z\,\psi_y(x,y) + z^2\xi_y(x,y) + z^3\,\zeta_y(x,y) \quad (3)$$
$$w(x,y,z) = w_0(x,y)$$

(u_0, v_0, w_0) denote the displacements of a point (x, y) on the midplane, and (ψ_x, ψ_y) are the rotations of normals to midplane about the Y and X-axes, respectively. TSDT models are implemented in FGP thermo-mechanical buckling analysis in [26, 76-78] for rectangular FGPs and in [30] for skew FGP.

Reddy's TSDT is a TSDT in which the functions $(\xi_x, \xi_y, \zeta_x, \zeta_y)$ are determined using the condition that the transverse shear stresses at the top and bottom surfaces are zero. By finding $(\psi_x, \psi_y, \xi_x, \xi_y, \zeta_x, \zeta_y)$, Reddy's TSDT displacement field reduced to Eq. (4).

$$\begin{aligned} u(x,y,z) &= u_0(x,y) + z\,\phi_x(x,y) - \frac{4z^3}{3h^2}\left(\phi_x + \frac{\partial \omega_0}{\partial x}\right) \\ v(x,y,z) &= v_0(x,y) + z\,\phi_y(x,y) - \frac{4z^3}{3h^2}\left(\phi_y + \frac{\partial \omega_0}{\partial y}\right) \\ w(x,y,z) &= w_0(x,y) \end{aligned} \tag{4}$$

(ϕ_x, ϕ_y) denote slopes of a transverse normal at the neutral plane. Reddy's TSDT models are implemented in FGP thermo-mechanical buckling analysis only for rectangular FGP in [27, 35-38, 41, 44-47, 49, 54, 79, 80].

3.2.4. Non-polynomial shear deformation theories (Non-polynomial SDTs)

This is a category of shear deformation theories, in which the proposed displacement fields are not in polynomial form; instead, they may be in trigonometric, hyperbolic or any other non-polynomial form. In literature of thermo-mechanical buckling analysis of FGP, the only used non-polynomial SDTs is hyperbolic SDT in [43] for a rectangular FGP.

3.2.5. Four-variable shear deformation theories (Refined SDTs)

In plate theories (CPT, FSDT, TSDT, Trigonometric SDT, Hyperbolic SDT) there are five variables to find in order to solve the plate problem. These variables are u_0, v_0, w_0, ϕ_x and ϕ_y. In order to simplify the problem, number of variables can be reduced to only four variables by splitting $w(x, y, z)$ to two parts (w_b, w_s), and express the inplane displacements as functions of these two parts as shown in Eq. (5).

$$\begin{aligned} u(x,y,z) &= u_0(x,y) - z\frac{\partial w_b}{\partial x} - f(z)\frac{\partial w_s}{\partial x} \\ v(x,y,z) &= v_0(x,y) - z\frac{\partial w_b}{\partial y} - f(z)\frac{\partial w_s}{\partial y} \\ w(x,y,z) &= w_b(x,y) + w_s(x,y) \end{aligned} \tag{5}$$

w_b , w_s are the bending and shear components of transverse displacement. Now there are just four variables to find u_0, v_0, w_b and w_s. This refinement, i.e. variables reduction, can be applied

to any shear deformation theory. In literature of thermo-mechanical buckling analysis of FGP, only Bateni [42] used the four-variable refined SDT.

3.3.Von-Karman nonlinearities

Von Karman nonlinearities are commonly used assumptions that consider simplified nonlinearity by assuming small strain with moderate rotation, aka moderately large deformation assumption [58, 62]. In literature, Von Karman nonlinearities are also called Geometrical nonlinearity or kinematic nonlinearities, and it is commonly considered in thermo-mechanical buckling analysis of FGPs. When Von Karman introduced to CPT it can be referred to as CPT with Von Karman nonlinearities, or Von Karman plate theory.

4. Properties characterization of FGP

Properties of FGP at any point can be specified using function models or micromechanics models. Following is a brief on the characterization methods those are used in the literature of FGP thermo-mechanical buckling analysis.

4.1. Function models

Microstructure of FGP changes continuously, through at least one dimension, from one composition to another. This change may be designed to have any function. Function models may directly describe properties variation or just the microstructure variation, i.e. volumetric ratios of each component. The common functions used in modelling FGPs are listed below.

4.1.1 Power function model

Power function model is the most commonly used function in FGP studies. Functionally graded materials that obey power function rule are called (P-FGM). The power function expresses directly property variation or volume fraction change. If it describes the volume fraction change then a micromechanical model, e.g. Voigt, Mori-Tanaka…, is needed to obtain the distributed properties. Power law expressing volume fraction through FGP may have the form of Eq. (6), presented by Amoushahi [65] considering the coordinate system shown in Fig. 6.

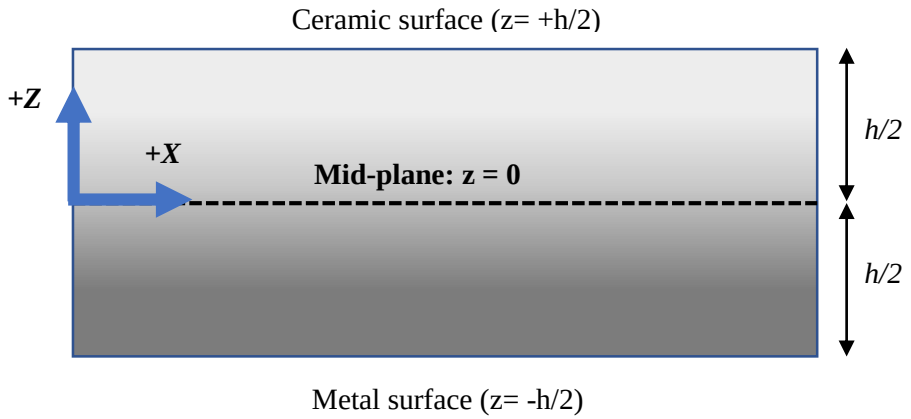

Fig. 6 FGP's cross section and coordinate system

$$v_c(z) = \left(\frac{1}{2} + \frac{z}{h}\right)^n, \qquad \frac{-h}{2} \le z \le \frac{h}{2} \tag{6}$$

$v_c(z)$ is the volumetric fraction of ceramic at plane (z), n is the power index value. Note that if the power index n is zero, then the plate will be homogenous plate. If the power index is 1, then the variation will be linear. At $z = +h/2$ the material is pure ceramic, $v_c(h/2) = 1$. Also at $z = -h/2$ the material is pure metal $v_c(-h/2) = 0$.

4.1.2 Sigmoid function model

Functionally graded materials that obey sigmoid power function rule are called (S-FGM) or (S-P-FGM). Sigmoid power function is the combination of two different power functions, one for positive range of z and one for the negative range of z. Sigmoid power function is used to obtain volume fraction v_c, then a micromechanical approach, e.g. Voigt, Mori-Tanaka… is used to obtain the distributed properties. Sigmoid power model ensures smooth distribution of the resulting stress [59, 81]. An example of sigmoid power function is shown in Eq. (7) that is found in [76] considering the coordinate system shown in Fig. 6.

$$v_c(z) = \begin{cases} \left(\frac{1}{2} + \frac{z}{h}\right)^n, & \frac{-h}{2} \le z \le 0 \\ \left(\frac{1}{2} - \frac{z}{h}\right)^n, & 0 \le z \le \frac{h}{2} \end{cases} \tag{7}$$

Sigmoid power function model is rarely used in modeling FGP for thermo-mechanical buckling analysis. Specifically, it has been implemented just by Duc [76] and Chikh [43].

4.2. Micromechanics models

Aim of these methods is to predict the effective properties of a composite at given point or lamina as a function of the material and geometric of the composite microstructure using the volumetric ratios obtained by a function model. Daniel [82] categorized these methods as follows.

4.2.1 Mechanics of materials methods

These methods are made simple by assuming uniform strain (parallel, rule of mixture, Voigt model) or uniform stress (series, inverse rule of mixture, Reuss model) [82]. Both of them are shown in Eq. (8).

$$\begin{aligned} &Voigt\ model\ (Rule\ of\ mixture):\ C^* = v_c C_c + v_m C_m = v_c C_c + (1 - v_c) C_m \\ &Ruess\ model\ (Inverse\ rule\ of\ mixture):\ C^* = \frac{1}{\frac{v_c}{C_c} + \frac{v_m}{C_m}} = \frac{1}{\frac{v_c}{C_c} + \frac{(1 - v_c)}{C_m}} \end{aligned} \tag{8}$$

C^* is the effective property, C_c, C_m are properties of the consistent, v_c, v_m are their volume fractions. Voigt model is the most popular in studies of FGP thermo-mechanical buckling analysis.

4.2.2 Theory of elasticity methods

Applies theory of elasticity on a simplified model, resulting in close-form solutions for elastic properties. Common methods are self-consistent methods (effective medium approximation) and Mori-Tanaka method (effective field approximation) [82]. Self-consistent method is used when a crack introduced to the problem [83]. Mori-Tanaka method is used to count for randomness of particulates distribution in a continuous phase [19]. In the literature of thermo-mechanical buckling analysis of FGPs, Fan [38] used the self-consistent model; and Taj [30] and Sharma [69, 70] used Mori-Tanaka model.

4.2.3 Semi-empirical methods

Use simple interpolation between bounds obtained by micromechanics methods, while giving comparatively better results [82]. The most common semi-empirical method is Halpin-Tsi method. In the literature of FGP thermo-mechanical buckling analysis, Halpin-Tsai model has been implemented by Yu [44] and Wu [71].

5. Buckling

Buckling of a plate can be defined as the loss of its stability under compressive loading [84]. That is, the shape of the buckled structure changes into a different configuration when the loads reach some critical value. Buckling occurrence depends on the shape of the structure, properties of the material, loading configuration and boundary conditions. Different bodies buckles in different ways. Columns and flat plates experience bifurcation buckling, aka classical buckling; while curved plates experience snap-through buckling and cylindrical shells experience finite disturbance buckling [62].

5.1. Stability equation

Stability equations are the equations derived to obtain buckling loads and their associated mode shapes. Approaches used to obtain stability equations are minimum total potential energy approach, and linear equations approach.

In the first approach, equilibrium equations are derived based on the principle of minimum total potential energy, and then solved for minimum buckling load. Most of studies in literature use this approach in detecting instability.

The second approach is called linear equations approach, which yields stability equations as linear ordinary differential equations, which are easy to solve. This group contains Trefftz criterion and adjacent equilibrium criterion. According to the Trefftz, aka Minimum Potential Energy Difference, criterion, a structure is in a configuration of stable equilibrium if and only if positive change in total potential energy occurs corresponding to any sufficiently small and kinematically admissible displacement. In the literature of FGP thermo-mechanical buckling analysis, Shariyat [29] used Trefftz criterion in detecting instability of perforated FG annular sector plates modeled using 3D elasticity theory. The second approach in the group of linear equation approach is adjacent (neighboring) equilibrium criterion, which considers the equilibrium configuration at the buckling (bifurcation) point and an adjacent configuration that is very close just after buckling point [84]. Many published works used this method, examples can be found at [39, 42, 50].

5.2. FGP buckling

Aydogdu [85] studied the conditions for bifurcation buckling to exist in the case of FGPs; concluding that for unsymmetrical FGP, under only in-plane compression load, bifurcation can only occur when all edges are clamped. That is because in-plane (stretching) and out-plane (bending) displacements are coupled, just like the case of unsymmetrical laminated plates [62]. Therefore, in-plane load, if even one edge of the unsymmetrical FGP is simply supported the plate will bend. Under uniform shear load bifurcation can occur at plates with clamped as well as simply supported edge, since both of these boundary conditions provide twisting resistance. The stability problem of functionally graded plates is very sensitive to the type of boundary conditions and the form of material variation across the plate thickness. In order for bifurcation point (buckling load) to exist at plate under in-plane compression, initial flatness is necessary. That is, plate has to be initially flat and has to stay flat until buckling occurs. Otherwise, it will not arrive to the bifurcation point, and just exhibits bending deformation. Initial flatness may be interrupted not only by in-plane loads with unclamped boundary conditions, but also by initial imperfections in the structure. Under biaxial in-plane compression, if loads suitably selected, in-plane strain may vanish, then bifurcation point will occur on simply supported plates even if the plate is non-symmetric. Pre-buckling status, i.e. stress and strain, has to studied before conducting buckling studies [62]. An attempt to decouple the stretching and bending deformations, in-plane loads/boundary conditions made to act on the physical neutral plane [86]. Physical neutral plane is the plane that has neither stress nor strain under pure bending. According to Zhang [87] using coordinate system shown in

Fig. 7, the discrepancy between the physical neutral plane and the mid-plane (C) can be calculated using the relation in Eq. (9). In Eq. (9) $E(z)$ is the function that describes the variation of the elasticity module through the thickness of the plate. Note that if the plate is homogeneous, i.e. $E(z) = const.$, C will vanish and the two planes will coincide on each other.

$$C = \int_{-\frac{h}{2}}^{+\frac{h}{2}} E(z)\, z\, dz \Big/ \int_{-\frac{h}{2}}^{+\frac{h}{2}} E(z)\, dz \tag{9}$$

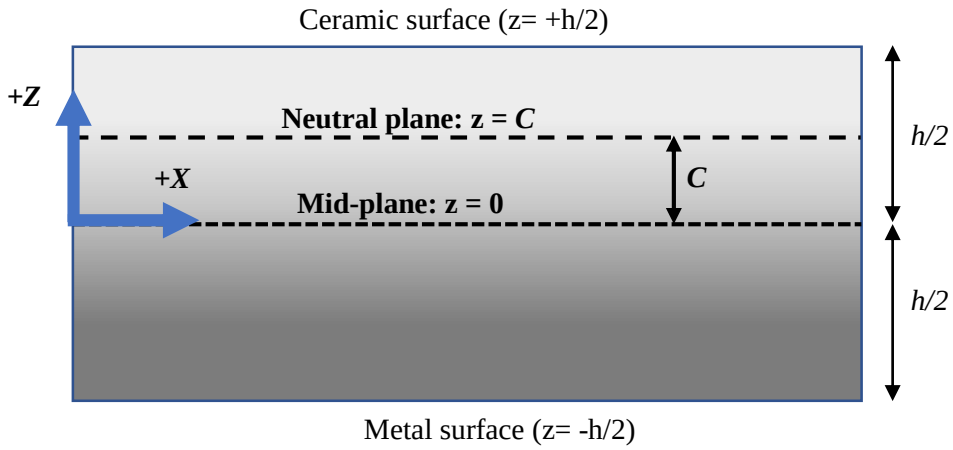

Fig. 7 Neutral and mid planes of FGP

Initial geometry imperfections have been considered in many published studies. Normally initial imperfections are introduced to the analysis as pre-existing lateral deformation. Recent articles that consider initial imperfections are [25, 37, 79].

5.3. FGP thermal buckling

Temperature generates in-plane compression load between every two opposite inextensible edges. If the neutral plane is assumed to be coincident with the mid-plane of non-symmetrical FGP under thermal load, all edges has to be clamped in order to bifurcation point to occur [88]. If all edges are free to expand, i.e. movable, there will be no in-plane thermal stress and the temperature effect will be only on properties of the materials. For symmetrical FGP, if the plate is initially flat, it remains flat until bifurcation point occurs. Initiation of lateral deflection under the applied load, below bifurcation point, results into the plate bending and the bifurcation never occurs, instead of that, it becomes a bending problem. This condition occurs when a rectangular FGP with simply supported boundary conditions is under thermal load, provided that the material distribution across the plate thickness is not symmetric with respect to plate's mid-plane unless physical neutral plane is considered [62, 85]. Swaminathan [19] presented a comprehensive review on thermal analysis of FGPs.

5.4. Thermal loads

Thermal loads applied on a FGP can be expressed by constant or changing temperature through one dimension or more. Temperature variation may be given directly as a spatial function or derived from heat conduction problem. Temperature variation equation, normally through thickness, may be a constant, e.g. [68, 89], linear, e.g. [89, 90] or nonlinear equation, e.g. [34, 80]. Temperature variation may be also given as heat conduction problem as in [32, 33, 42, 49, 91].

5.5. Temperature-dependent FGP

Thermal load does not just generate stresses in the structure, it also affect the structure's material properties. Considering this effect of temperature rises the complexity level of the analysis. In the literature on FGP thermo-mechanical buckling, temperature-dependency effect on the analysis results has been studied by Shukla [68], Lal [80] and Jari [78] by comparing results of analysis with and without considering martial properties dependency on temperature. Other studies those considered temperature-dependent material properties are [24, 25, 27, 30, 32, 35, 38, 42, 45, 48, 49, 53, 66, 69, 70, 72, 76, 77, 92]. Examples of studies those considered temperature-independent material properties are [22, 23, 26, 29, 36, 41, 50, 65].

5.6. FGP thermo-mechanical buckling

FGP, as functionally graded materials, are expected to withstand highly elevated temperature without failure. Normally, in addition to the thermal loads there are mechanical loads acting. In that case, the FGP has to withstand both the thermal and mechanical loads at the same time. There is a huge amount of published works deal with mechanical buckling or/and thermal buckling of FGP separately, but small amount of them treat the thermo-mechanical buckling case as defined here as buckling due to simultaneous application of thermal and mechanical loads. This situation is complicated enough so that until now no exact solution available even for the simplest configuration possible. Existence of bifurcation point has to be examined through the analysis of pre-buckling state of the plate. Zhang [92] and Kowal-Michalska [22] attempted to apply the concept of physical neutral plane.

6. Solution procedures

There are many solution methods have been applied in various FGP analysis problems. Solution methods can be categorized as exact, semi analytical and approximate methods. However, only approximate methods have been applied to solve the thermo-mechanical buckling of FGP. Approximate methods contain two main categories, approximately analytical methods and numerical methods. Many methods fall under this category. However only few have been applied to solve the buckling of FGP under combined thermal and mechanical loads.

6.1. Approximate analytical methods

These methods seek to obtain approximate solution as a function. This group contains the following methods.

6.1.1 Ritz method

Ritz method is a simple and convenient method based on the principle of minimum potential energy. In literature of thermo-mechanical buckling of FGPs it is found that Ritz method has been used in snap-through buckling of thermally post-buckled plate analyses by: Kiani [32], who analyzed static and dynamic case for circular FGPs using Ritz method with Gram-Schmidt process; and Zhang [92], who analyzed the static case of rectangular FGP using multi-term Ritz method.

6.1.2 Galerkin method

Galerkin method is a special case of the weighted residual method. This method deals with the governing differential equation directly instead of the energy functional. Therefore, Galerkin method is more general than Ritz method [58]. Galerkin method is one of the most commonly used methods in analyzing thermo-mechanical buckling of FGPs. Duc and various co-authors investigated thermo-mechanical buckling and post-buckling of FGPs based on: CPT [66], FSDT [24, 53] and Reddy's TSDT [26, 41]. Other researchers also presented thermo-mechanical buckling analysis of symmetric FGPs [43, 76], stiffened FGPs [25, 27, 35], porous FGPs [37], square FGP based on CLPT [22] and rectangular FGP based on four-variable refined plate theory by using multi-term Galerkin method [42].

6.1.3 Perturbation methods

Perturbation methods can solve various boundary-value problems in elastic structures[93], by starting from the exact solution of a related, simpler problem. There are main two versions of this method: traditional and two-step perturbation methods. Fallah [67] compared the two variations of this method, i.e. one- and two- step perturbation method, for nonlinear analysis of FGP with thermo-mechanical loading, and concluded that the two-step method must be used instead of the one-step method. Fellah [33] also applied two-step perturbation method to investigate thermo-mechanical buckling of circular FGP. This method is the most used one in analysis of thermo-mechanical buckling of FGPs. Shen and his various co-authors used two-step perturbation method repeatedly to investigate thermo-mechanical buckling and post-buckling of various continuous, laminated and sandwich FG reinforced plates, with or without elastic foundation [44, 46, 49, 54, 79] in various thermal environments, and in hygrothermal environment [45]. Fan [38] used two-perturbation method to investigate thermo-mechanical buckling of cracked FG reinforced plate.

6.1.4 Power series Frobenius method

This method aims to find an infinite series solution for ordinary differential equations. Yaghoobi [50] used this method to obtain approximate analytical solution for the ordinary differential equations those have been reduced analytically from the governing equations of stability to investigate thermo-mechanical buckling of FGP.

6.1.5 Fast converging finite double Chebyshev series

In this method, displacement functions and loading are approximated in space domain by finite degree double Chebyshev polynomials. This method used by Shukla [68] to investigate thermo-mechanical post-buckling of FGP.

6.2. Numerical methods

Numerical methods obtain approximate solution as a value at many points of the solution domain. These methods are used in order to avoid difficulties associated with the analytical solution methods [56].

6.2.1 Finite element methods (FEM)

Finite element method is a powerful method used in solving differential equations those describe engineering systems. The concept behind these methods is that they divide the problem domain into smaller simpler geometric shapes; so they deal with the problem of interest as assemblage of sub-problems those are simpler and easier to solve [20]. FEMs have been used in the analysis of thermo-mechanical buckling of FGPs based on various theories. Following, FEM implementations are categorized based on the considered model of the FGP.

Based on various plate theories (e.g. FSDT, TSDT): Recently, Moita [94] used FEM based on Reddy's TSDT, to compare between linear and nonlinear mechanical and thermo-mechanical buckling of rectangular FGP. FEM has been also used in investigation of thermo-mechanical buckling of: rectangular FGPs by Talha [77], skew FGPs by Taj [30], rectangular FGP with an elliptical cutout by Abolghasemi [73], and sandwich FGPs by Chen [95]. Lal and co-authors investigated stochastic thermo-mechanical buckling and post-buckling of FGPs with holes [36], and further included temperature dependency [80]. Sharma imbedded elasto-plasticity to the thermo-mechanical buckling and post-buckling investigation of FGPs with cutout [70] and further included temperature dependency [69]. Mania [23] investigated the dynamic thermo-mechanical buckling in addition to the static buckling. Recently, Correia [96] conducted multi-objective optimization study including buckling analysis of thermo-mechanical loading for FGP using FEM.

Based on theory of elasticity: Shariyat [29] investigated the thermo-mechanical buckling of perforated annular sector using curved 3D B-splined C2-continuous element.

Many commercial finite element packages provide the ability to model FGPs based on both plate theories and 3D elasticity theory. Discussion of these packages is out of the scope of this review. However, detailed illustration to model and conduct buckling analysis of rectangular plates including FGPs using models based on FSDT and 3D elasticity theory using ANSYS® APDL [97] is provided by Hassan [98].

6.2.2 Finite strip methods (FSM)

FSM is a variation of the finite element method, where elements are long strips laid parallel to one another to form the plate [65]. Functionally graded finite strip element is made of mixture of metal and ceramic [99]. This method has many variations depending on the proposed basis shape functions, one of which is the complex finite strip method, which is used by Amoushahi [65] to analysis thermo-mechanical buckling of FGPs.

6.2.3 Isogeometric analysis (IGA)

IGA is an integration of spline-based Computer Aided Design (CAD) with finite element method FEM into a single model [78, 100]. IGA bases geometry and solution on same spline function, which makes it easy to have exact description of geometrical complexities [31]. IGA usually based on Non-Uniform Rational B-Spline (NURBS). NURBS-based IGA has been applied by Jari [78] and Yu [31] in the analysis of the thermo-mechanical buckling of FGPs.

6.2.4 Differential quadrature method (DQM)

DQM approximates the partial derivative of a function at a given discrete point as a weighted linear combination of the function values at all the discrete points of the domain [72]. The key to implement DQM is to determine the weighting coefficients [101]. This method is used in investigating the dynamic thermo-mechanical buckling of FGP by Yang [72] and Wu [71]. Mansouri used new DQM that was proposed by Wang [102] to investigate thermo-mechanical buckling of: orthotropic FGPs [103] and orthotropic FGP on elastic foundation in thermal and moisture environment [47].

6.2.5 Meshless method

Meshless methods do not require connected nodes. These promising methods continue to improve and get more attention and implementations in engineering field [81, 104, 105]. This category includes wide range of subcategories. Shams [48] used Element-Free Galerkin (EFG) method to investigate thermo-mechanical buckling of FGP.

6.2.6 Shooting method

Shooting method solves boundary value problem after converting it to initial value problem, using trial initial conditions and interpolations in order to correct the initial condition until final condition be satisfied [105]. Shooting method has been used in investigating thermo-mechanical buckling of circular FGP by Li [34].

7. Concluding remarks and future direction

The present study presents a review on literature of modelling techniques and solution methods for the thermo-mechanical buckling of functionally graded plates. Following conclusions can be drawn based on the literature reviewed.

There is no publication found to obtain exact elasticity solution or even semi-analytical solution for the FGP buckling under combined thermal and mechanical loads.

Mostly used methods are Galerkin method, Perturbation method and finite element method. Just few solution methods used in this field of analysis. Many other numerical and approximate analytical methods can be implemented and compared with the available results in the literature.

Rectangular FGPs are the mostly studied; circular FGPs get less attention and skew FGPs are rare in this field. Other general shape of plates are not even exist in this literature.

Stiffened, perforated and cracked FGPs have minimum attention in this field of analysis.

FGP models based on elasticity are rare in this literature. Models based on plate theories are more common.

Relatively new plate models, as Carrera's unified formulation CUF [106], have not implemented yet in this field of study.

Dynamic thermo-mechanical buckling of FGP is a missing topic.

Most of the reported researches include post-buckling study along with the buckling study. Many studies consider the combined thermal and mechanical load only in the post-buckling study, but not in the buckling study. These studies are excluded from this review.

Existing gaps found in the literature of the thermo-mechanical buckling analysis of FGP, offer many chances to contribute. Implementation of the already used solution methods but for other models of FGP, implementation of never used solution methods, obtaining an exact solution for any FGP configuration and implementation of CUF model are suggested topics for future researches.

This review aimed at stimulating researchers to contribute to this field of study, so better analysis tools will be available to designers to make maximum benefit from the promising FGM concept.

References

[1] Birman, V., Keil, T., Hosder, S., *Functionally graded materials in engineering*, in *Structural Interfaces and Attachments in Biology*, Springer New York, 19-41, 2013.

[2] Shen, M., Bever, M., Gradients in polymeric materials. *Journal of Materials science*, 7(7), 741-746, 1972.

[3] Bever, M., Duwez, P., Gradients in composite materials. *Materials Science and Engineering*, 10, 1-8, 1972.

[4] Singh, A.K., Noise Emission form Functionally Graded Materials based Polypropylene Spur Gears-A Tribological Investigation. *Materials Today: Proceedings*, 5(2), 8199-8205, 2018.

[5] Singh, A.K., A novel technique for in-situ manufacturing of functionally graded materials based polymer composite spur gears. *Polymer Composites*, 40(2), 523-535, 2019.

[6] Tian, X., Zhao, J., Yang, H., Wang, Z., Liu, H., High-speed intermittent turning of GH2132 alloy with Si 3 N 4/(W, Ti) C/Co graded ceramic tool. *The International Journal of Advanced Manufacturing Technology*, 100(1-4), 401-408, 2019.

[7] Ngueyep, L.L.M., Ndop, J., Nkene, E.R.A., Ndjaka, J.-M.B., Numerical and Analytical Calculations for Modeling and Designing Drilling Wicks or Rotary Cutters Based of Functionally Graded Materials. *Journal of Engineering*, 2018, 2018.

[8] Nikbakht, S., Kamarian, S., Shakeri, M., A review on optimization of composite structures Part II: Functionally graded materials. *Composite Structures*, 2019.

[9] Hayakawa, N., Oishi, R., Kojima, H., Kato, K., Zebouchi, N. Electric Field Grading by Functionally Graded Materials (FGM) for HVDC Gas Insulated Power Apparatus. *IEEE Conference on Electrical Insulation and Dielectric Phenomena (CEIDP)*, IEEE, 2018.

[10] Radhi, N., Hafiz, M., Atiyah, A., Preparation and Investigation of Corrosion and Biocompatibility Properties for Functionally Graded Materials (NiTi). *Ind Eng Manage S*, 3, 2169-0316, 2018.

[11] Radhi, N., Preparation And Modeling (Titanium-Hydroxyapatite) Functionally Graded Materials For Bio-Medical Application. *International Journal of Civil Engineering and Technology (IJCIET)*, 9(6), 28-39, 2018.

[12] Dabbagh, A., Madfa, A., Naderi, S., Talaeizadeh, M., Abdullah, H., Abdulmunem, M., Kasim, N.A., Thermomechanical advantages of functionally graded dental posts: A finite element analysis. *Mechanics of Advanced Materials and Structures*, 1-10, 2017.

[13] Mahmoudi, M., Saidi, A.R., Hashemipour, M.A., Amini, P., The use of functionally graded dental crowns to improve biocompatibility: a finite element analysis. *Computer methods in biomechanics and biomedical engineering*, 21(2), 161-168, 2018.

[14] Satapathy, P.K., Sahoo, B., Panda, L., Das, S. Finite element analysis of functionally graded bone plate at femur bone fracture site. *IOP Conference Series: Materials Science and Engineering*, IOP Publishing, 2018.

[15] Han, C., Li, Y., Wang, Q., Wen, S., Wei, Q., Yan, C., Hao, L., Liu, J., Shi, Y., Continuous functionally graded porous titanium scaffolds manufactured by selective laser melting for bone implants. *Journal of the mechanical behavior of biomedical materials*, 80, 119-127, 2018.

[16] Kumar, G.M. Functionally graded bio-ceramic reinforced PVA hydrogel composites for knee joint artificial cartilages. *AIP Conference Proceedings*, AIP Publishing, 2018.

[17] Cooley, W.G., Application of functionally graded materials in aircraft structures, in Department of Aeronautics and Astronautics. 2005, Air University.

[18] Swaminathan, K., Naveenkumar, D.T., Zenkour, A.M., Carrera, E., Stress, vibration and buckling analyses of FGM plates: A state of the art review. *Composite Structures*, 120, 10-31, 2015.

[19] Swaminathan, K., Sangeetha, D.M., Thermal analysis of FGM plates – A critical review of various modeling techniques and solution methods. *Composite Structures*, 160, 43-60, 2017.

[20] Reddy, J.N., *Theory and analysis of elastic plates and shells*; CRC press, 2006.

[21] Ventsel, E., Krauthammer, T., *Thin plates and shells: theory: analysis, and applications*; CRC press, 2001.

[22] Kowal-Michalska, K., Mania, R.J., Static and dynamic thermomechanical buckling loads of functionally graded plates. *Mechanics and Mechanical Engineering*, 17(1), 99-112, 2013.

[23] Mania, R.J. Dynamic response of FGM thin plate subjected to combined loads. *10th Jubilee Conference on "Shell Structures: Theory and Applications", SSTA*, Gdansk, 2013.

[24] Tung, H.V., Thermal and thermomechanical postbuckling of FGM sandwich plates resting on elastic foundations with tangential edge constraints and temperature dependent properties. *Composite Structures*, 131, 1028-1039, 2015.

[25] Cong, P.H., Ngoc An, P.T., Duc, N.D., Nonlinear stability of shear deformable eccentrically stiffened functionally graded plates on elastic foundations with temperature-dependent properties. *Science and Engineering of Composite Materials*, 24(3), 455-469, 2017.

[26] Bakora, A., Tounsi, A., Thermo-mechanical post-buckling behavior of thick functionally graded plates resting on elastic foundations. *Structural Engineering and Mechanics*, 56(1), 85-106, 2015.

[27] Duc, N.D., Cong, P.H., Quang, V.D., Thermal stability of eccentrically stiffened FGM plate on elastic foundation based on Reddy's third-order shear deformation plate theory. *Journal of Thermal Stresses*, 39(7), 772-794, 2016.

[28] Aghazadeh, R., Dag, S., Cigeroglu, E., Thermal effect on bending, buckling and free vibration of functionally graded rectangular micro-plates possessing a variable length scale parameter. *Microsystem Technologies*, 1-24, 2018.

[29] Shariyat, M., Behzad, H., Shaterzadeh, A.R., 3D thermomechanical buckling analysis of perforated annular sector plates with multiaxial material heterogeneities based on curved B-spline elements. *Composite Structures*, 188, 89-103, 2018.

[30] Taj, M.N.A.G., Chakrabarti, A., Buckling analysis of functionally graded skew plates: An efficient finite element approach. *International Journal of Applied Mechanics*, 5(4), 2013.

[31] Yu, T., Yin, S., Bui, T.Q., Liu, C., Wattanasakulpong, N., Buckling isogeometric analysis of functionally graded plates under combined thermal and mechanical loads. *Composite Structures*, 162, 54-69, 2017.

[32] Kiani, Y., Axisymmetric static and dynamics snap-through phenomena in a thermally postbuckled temperature-dependent FGM circular plate. *International Journal of Non-Linear Mechanics*, 89, 1-13, 2017.

[33] Fallah, F., Nosier, A., Nonlinear behavior of functionally graded circular plates with various boundary supports under asymmetric thermo-mechanical loading. *Composite Structures*, 94(9), 2834-2850, 2012.

[34] Li, S.R., Zhang, J.H., Zhao, Y.G., Nonlinear thermomechanical post-buckling of circular FGM plate with geometric imperfection. *Thin-Walled Structures*, 45(5), 528-536, 2007.

[35] Van Dung, D., Nga, N.T., Buckling and postbuckling nonlinear analysis of imperfect FGM plates reinforced by FGM stiffeners with temperature-dependent properties based on TSDT. *Acta Mechanica*, 227(8), 2377-2401, 2016.

[36] Lal, A., Neeranjan Singh, H., Shegokar, N.L., FEM model for stochastic mechanical and thermal postbuckling response of functionally graded material plates applied to panels with circular and square holes having material randomness. *International Journal of Mechanical Sciences*, 62(1), 18-33, 2012.

[37] Cong, P.H., Chien, T.M., Khoa, N.D., Duc, N.D., Nonlinear thermomechanical buckling and post-buckling response of porous FGM plates using Reddy's HSDT. *Aerospace Science and Technology*, 77, 419-428, 2018.

[38] Fan, Y., Wang, H., Nonlinear bending and postbuckling analysis of matrix cracked hybrid laminated plates containing carbon nanotube reinforced composite layers in thermal environments. *Composites Part B: Engineering*, 86, 1-16, 2016.

[39] Mahmoudi, A., Benyoucef, S., Tounsi, A., Benachour, A., Adda Bedia, E.A., Mahmoud, S.R., A refined quasi-3D shear deformation theory for thermo-mechanical behavior of functionally

graded sandwich plates on elastic foundations. *Journal of Sandwich Structures and Materials*, 2017.

[40] Shahsavari, D., Shahsavari, M., Li, L., Karami, B., A novel quasi-3D hyperbolic theory for free vibration of FG plates with porosities resting on Winkler/Pasternak/Kerr foundation. *Aerospace Science and Technology*, 72, 134-149, 2018.

[41] Duc, N.D., Van Tung, H., Mechanical and thermal postbuckling of higher order shear deformable functionally graded plates on elastic foundations. *Composite Structures*, 93(11), 2874-2881, 2011.

[42] Bateni, M., Kiani, Y., Eslami, M.R., A comprehensive study on stability of FGM plates. *International Journal of Mechanical Sciences*, 75, 134-144, 2013.

[43] Chikh, A., Bakora, A., Heireche, H., Houari, M.S.A., Tounsi, A., Adda Bedia, E.A., Thermo-mechanical postbuckling of symmetric S-FGM plates resting on Pasternak elastic foundations using hyperbolic shear deformation theory. *Structural Engineering and Mechanics*, 57(4), 617-639, 2016.

[44] Yu, Y., Shen, H.S., Wang, H., Hui, D., Postbuckling of sandwich plates with graphene-reinforced composite face sheets in thermal environments. *Composites Part B: Engineering*, 135, 72-83, 2018.

[45] Shen, H.S., Zhang, C.L., Non-linear analysis of functionally graded fiber reinforced composite laminated plates, Part I: Theory and solutions. *International Journal of Non-Linear Mechanics*, 47(9), 1045-1054, 2012.

[46] Shen, H.S., Zhu, Z.H., Postbuckling of sandwich plates with nanotube-reinforced composite face sheets resting on elastic foundations. *European Journal of Mechanics, A/Solids*, 35, 10-21, 2012.

[47] Mansouri, M.H., Shariyat, M., Biaxial thermo-mechanical buckling of orthotropic auxetic FGM plates with temperature and moisture dependent material properties on elastic foundations. *Composites Part B: Engineering*, 83, 88-104, 2015.

[48] Shams, S., Soltani, B., Memar Ardestani, M., The effect of elastic foundations on the buckling behavior of functionally graded carbon nanotube-reinforced composite plates in thermal environments using a meshfree method. *Journal of Solid Mechanics*, 8(2), 262-279, 2016.

[49] Shen, H.S., Li, S.R., Postbuckling of sandwich plates with FGM face sheets and temperature-dependent properties. *Composites Part B: Engineering*, 39(2), 332-344, 2008.

[50] Yaghoobi, H., Yaghoobi, P., Buckling analysis of sandwich plates with FGM face sheets resting on elastic foundation with various boundary conditions: An analytical approach. *Meccanica*, 48(8), 2019-2035, 2013.

[51] Hussein, O.S., Mulani, S.B. Two-dimensional optimization of functionally graded material plates subjected to buckling constraints. *58th AIAA/ASCE/AHS/ASC Structures, Structural Dynamics, and Materials Conference*, American Institute of Aeronautics and Astronautics Inc, AIAA, 2017.

[52] Demirbas, M.D., Apalak, M.K., Thermal stress analysis of one- and two-dimensional functionally graded plates subjected to in-plane heat fluxes. *Proceedings of the Institution of Mechanical Engineers, Part L: Journal of Materials: Design and Applications*, 2017.

[53] Duc, N.D., Tung, H.V., Mechanical and thermal postbuckling of shear-deformable FGM plates with temperature-dependent properties. *Mechanics of Composite Materials*, 46(5), 461-476, 2010.

[54] Shen, H.S., Zhu, Z.H., Buckling and postbuckling behavior of functionally graded nanotube-reinforced composite plates in thermal environments. *Computers, Materials and Continua*, 18(2), 155-182, 2010.

[55] Reddy, J.N., *Mechanics of laminated composite plates and shells: theory and analysis*; CRC press, 2004.

[56] Szilard, R., *Theories and applications of plate analysis: classical, numerical and engineering methods*; John Wiley & Sons, 2004.

[57] Jones, R.M., *Buckling of bars, plates, and shells*; Bull Ridge Corporation, 2006.

[58] Bhaskar, K., Varadan, T., *Plates: theories and applications*; John Wiley & Sons, 2014.

[59] Carrera, E., Fazzolari, F.A., Cinefra, M., *Thermal Stress Analysis of Composite Beams, Plates and Shells: Computational Modelling and Applications*; Academic Press, 2016.

[60] Chakraverty, S., Pradhan, K.K., *Vibration of functionally graded beams and plates*; Academic Press, 2016.

[61] Elishakoff, I., Pentaras, D., Gentilini, C., *Mechanics of functionally graded material structures*; World Scientific, 2016.

[62] Eslami, M.R., *Buckling and Postbuckling of Beams, Plates, and Shells*, 1; Springer, 2017.

[63] Thai, H.T., Kim, S.E., A review of theories for the modeling and analysis of functionally graded plates and shells. *Composite Structures*, 128, 70086, 2015.

[64] Abrate, S., Di Sciuva, M., Equivalent single layer theories for composite and sandwich structures: A review. *Composite Structures*, 179, 482-494, 2017.

[65] Amoushahi, H., Lajevardi, M.M., Buckling of functionally graded plates under thermal, axial, and shear in-plane loading using complex finite strip formulation. *Journal of Thermal Stresses*, 41(2), 182-203, 2018.

[66] Tung, H.V., Duc, N.D., Nonlinear analysis of stability for functionally graded plates under mechanical and thermal loads. *Composite Structures*, 92(5), 1184-1191, 2010.

[67] Fallah, F., Nosier, A., Sharifi, M., Ghezelbash, F., On perturbation method in mechanical, thermal and thermo-mechanical loadings of plates: Cylindrical bending of FG plates. *ZAMM Zeitschrift fur Angewandte Mathematik und Mechanik*, 96(2), 217-232, 2016.

[68] Shukla, K.K., Kumar, K.V.R., Pandey, R., Nath, Y., Postbuckling response of functionally graded rectangular plates subjected to thermo-mechanical loading. *International Journal of Structural Stability and Dynamics*, 7(3), 519-541, 2007.

[69] Sharma, K., Kumar, D., Elastoplastic stability and failure analysis of FGM plate with temperature dependent material properties under thermomechanical loading. *Latin American Journal of Solids and Structures*, 14(7), 1361-1386, 2017.

[70] Sharma, K., Kumar, D., Elastoplastic analysis of FGM plate with a central cutout of various shapes under thermomechanical loading. *Journal of Thermal Stresses*, 40(11), 1417-1441, 2017.

[71] Wu, H., Yang, J., Kitipornchai, S., Parametric instability of thermo-mechanically loaded functionally graded graphene reinforced nanocomposite plates. *International Journal of Mechanical Sciences*, 135, 431-440, 2018.

[72] Yang, S.F., Chen, H., Ran, C., Dynamic stability analysis of functionally graded plates subjected to complex loads, in 4th International Conference on Civil Engineering, Architecture and Building Materials, CEABM 2014. 2014, Trans Tech Publications Ltd: Haikou. p. 679-686.

[73] Abolghasemi, S., Shaterzadeh, A.R., Rezaei, R., Thermo-mechanical buckling analysis of functionally graded plates with an elliptic cutout. *Aerospace Science and Technology*, 39, 250-259, 2014.

[74] Reddy, J., A refined nonlinear theory of plates with transverse shear deformation. *International Journal of solids and structures*, 20(9-10), 881-896, 1984.

[75] Reddy, J., A general non-linear third-order theory of plates with moderate thickness. *International Journal of Non-Linear Mechanics*, 25(6), 677-686, 1990.

[76] Duc, N.D., Cong, P.H., Nonlinear postbuckling of symmetric S-FGM plates resting on elastic foundations using higher order shear deformation plate theory in thermal environments. *Composite Structures*, 100, 566-574, 2013.

[77] Talha, M., Singh, B.N., Thermo-mechanical buckling analysis of finite element modeled functionally graded ceramic-metal plates. *International Journal of Applied Mechanics*, 3(4), 867-880, 2011.

[78] Jari, H., Atri, H.R., Shojaee, S., Nonlinear thermal analysis of functionally graded material plates using a NURBS based isogeometric approach. *Composite Structures*, 119, 333-345, 2014.

[79] Shen, H.S., Xiang, Y., Lin, F., Hui, D., Buckling and postbuckling of functionally graded graphene-reinforced composite laminated plates in thermal environments. *Composites Part B: Engineering*, 119, 67-78, 2017.

[80] Lal, A., Jagtap, K.R., Singh, B.N., Post buckling response of functionally graded materials plate subjected to mechanical and thermal loadings with random material properties. *Applied Mathematical Modelling*, 37(5), 2900-2920, 2013.

[81] Sayyad, A.S., Ghugal, Y.M., Modeling and analysis of functionally graded sandwich beams: A review. *Mechanics of Advanced Materials and Structures*, 1-20, 2018.

[82] Daniel, I.M., Ishai, O., Daniel, I.M., Daniel, I., *Engineering mechanics of composite materials*, 3; Oxford university press New York, 1994.

[83] Laws, N., Dvorak, G.J., Hejazi, M., Stiffness changes in unidirectional composites caused by crack systems. *Mechanics of Materials*, 2(2), 123-137, 1983.

[84] Yoo, C.H., Lee, S., *Stability of structures: principles and applications*; Elsevier, 2011.

[85] Aydogdu, M., Conditions for functionally graded plates to remain flat under in-plane loads by classical plate theory. *Composite Structures*, 82(1), 155-157, 2008.

[86] Zhang, D.G., Zhou, Y.H., A theoretical analysis of FGM thin plates based on physical neutral surface. *Computational Materials Science*, 44(2), 716-720, 2008.

[87] Zhang, D.-G., Zhou, Y.-H., A theoretical analysis of FGM thin plates based on physical neutral surface. *Computational Materials Science*, 44(2), 716-720, 2008.

[88] Kiani, Y., Bagherizadeh, E., Eslami, M.R., Thermal buckling of clamped thin rectangular FGM plates resting on Pasternak elastic foundation (Three approximate analytical solutions). *ZAMM* -

Journal of Applied Mathematics and Mechanics / Zeitschrift für Angewandte Mathematik und Mechanik, 91(7), 581-593, 2011.

[89] Na, K.S., Kim, J.H. Three-dimensional thermomechanical buckling of functionally graded plates. *11th International Conference on Fracture, ICF11*, Turin, 2005.

[90] Najafizadeh, M.M., Hedayati, B., Refined theory for thermoelastic stability of functionally graded circular plates. *Journal of Thermal Stresses*, 27(9), 857-880, 2004.

[91] Na, K.S., Kim, J.H. Volume fraction optimization of functionally graded composite plates for stress reduction and thermo-mechanical buckling. *9th International Conference on Multiscale and Functionally Graded Materials, FGM IX*, Oahu Island, HI, 2008.

[92] Zhang, D.G., Zhou, H.M., Mechanical and thermal post-buckling analysis of FGM rectangular plates with various supported boundaries resting on nonlinear elastic foundations. *Thin-Walled Structures*, 89, 142-151, 2015.

[93] Shen, H.-S., *A two-step perturbation method in nonlinear analysis of beams, plates and shells*; John Wiley & Sons, 2013.

[94] Moita, J.S., Araújo, A.L., Correia, V.F., Soares, C.M.M., Herskovits, J., Buckling and nonlinear response of functionally graded plates under thermo-mechanical loading. *Composite Structures*, 2018.

[95] Chen, C.S., Liu, F.H., Chen, W.R., Vibration and stability of initially stressed sandwich plates with FGM face sheets in thermal environments. *Steel and Composite Structures*, 23(3), 251-261, 2017.

[96] Correia, V.M.F., Madeira, J.F.A., Araújo, A.L., Soares, C.M.M., Multiobjective optimization of functionally graded material plates with thermo-mechanical loading. *Composite Structures*, 207, 845-857, 2019.

[97] ANSYS® *Help System*. Mechanical APDL, ANSYS Parametric Design Language Guide. Release 17.1.

[98] Hassan, A.H.A., Kurgan, N., Modeling and Buckling Analysis of Rectangular Plates in ANSYS. *International Journal Of Engineering & Applied Sciences*, 11(1), 310-329, 2019.

[99] Ghannadpour, S.A.M., Ovesy, H.R., Nassirnia, M., An investigation on buckling behaviour of functionally graded plates using finite strip method, in 2012 International Conference on Mechanical Engineering and Materials, ICMEM 2012. 2012: Melbourne, VIC. p. 1470-1476.

[100] Lieu, Q.X., Lee, J., Lee, D., Lee, S., Kim, D., Lee, J., Shape and size optimization of functionally graded sandwich plates using isogeometric analysis and adaptive hybrid evolutionary firefly algorithm. *Thin-Walled Structures*, 124, 588-604, 2018.

[101] Liew, K.M., Huang, Y.Q., Bending and buckling of thick symmetric rectangular laminates using the moving least-squares differential quadrature method. *International Journal of Mechanical Sciences*, 45(1), 95-114, 2003.

[102] Wang, X., Tan, M., Zhou, Y., Buckling analyses of anisotropic plates and isotropic skew plates by the new version differential quadrature method. *Thin-Walled Structures*, 41(1), 15-29, 2003.

[103] Mansouri, M.H., Shariyat, M., Thermal buckling predictions of three types of high-order theories for the heterogeneous orthotropic plates, using the new version of DQM. *Composite Structures*, 113(1), 40-55, 2014.

[104] Chen, Y., Lee, J., Eskandarian, A., *Meshless methods in solid mechanics*; Springer Science & Business Media, 2006.

[105] Fasshauer, G.E., *Meshfree approximation methods with MATLAB*, 6; World Scientific, 2007.

[106] Carrera, E., Cinefra, M., Petrolo, M., Zappino, E., *Finite element analysis of structures through unified formulation*; John Wiley & Sons, 2014.